Book of Abstracts: CIHR Symposium on Novel Cancer Therapies and Innovations in Treatment Monitoring.
Sunnybrook Health Sciences Centre, Toronto, Onatario, Canada.
November 14-15, 2011
DOI: 10.7785/tcrt.2012.500298

Technology in Cancer Research and Treatment
ISSN 1533-0346
Volume 11, Number 5, October 2012

Apoptotic Ceramide Pathways and UGT8 Involvement in Response to a New Cancer Therapy Utilizing Ultrasound Activated Microbubbles

Azza Al-Mahrouki[1,2], William Tran[1,2], Gregory J. Czarnota[1,2]

[1]Imaging Research and Radiation Oncology, Sunnybrook Health Sciences Centre, Toronto, ON, Canada, M4N 3M5
[2]Departments of Radiation Oncology and Medical Biophysics, University of Toronto, Toronto, ON, Canada, M4N 3M5

E-mail: azza.almahrouki@sunnybrook.ca

***Introduction*:** Apoptosis is a form of cancer cell death that is triggered by a number of cancer therapies. Many complex pathways that initiate the apoptotic signal in response to therapy were previously investigated. However, the mechanisms that underlie such signal in microbubbles-based therapy were not yet elucidated.
***Materials and Methods*:** Here we used a number of *in vitro* and *in vivo* approaches that included gene analyses and transfer, histology, immunohistochemistry, clonogenic assays, as well as lipid analysis. These analyses were applied to a number of cell models that included HUVEC, PC3 and MCF-7.
***Results and Discussion*:** The microbubbles-based treatments were associated with an up-regulation of UGT8 gene. It codes for an enzyme, which catalyzes the formation of galactosyl ceramide (1, 2). The increased level was more profound in combined treatments of microbubbles and irradiation, and is thought to be a homeostatic mechanism to balance the increased levels of ceramide; a second messenger in apoptosis signaling. Furthermore, the partial silencing of UGT8 gene *in vivo* was associated with an increased level of ceramide in PC3 tumours. Additionally, combining microbubbles therapy with thermal therapy resulted in increased levels of ceramide in both PC3 and MCF-7 tumours. This supports the involvement of ceramide and UGT8 in the apoptotic signal, which is stimulated by the microbubble-based cancer therapy. Targeting such molecules can help in the optimization of this new therapy.

Key words: Apoptosis; Ceramide; UGT8; Ultrasound; Microbubbles.

1. Bosio, A., Binczek, E., Le Beau, M. M., Fernald, A. A., Stoffel, W. The human gene CGT encoding the UDP-galactose ceramide galactosyl transferase (cerebroside synthase): cloning, characterization, and assignment to human chromosome 4, band q26. *Genomics 34*(1), 69-75 (1996).
2. Mackenzie, P. I., Bock, K. W., Burchell, B., Guillemette, C., Ikushiro, S., Iyanagi, T., Miners, J. O., Owens, I. S., Nebert, D. W. Nomenclature update for the mammalian UDP glycosyltransferase (UGT) gene superfamily. *Pharmacogenet Genomics 15*(10), 677-85 (2005).

Improving the Lateral Resolution of Acoustic Microscopy Using Synthetic Aperture Reconstruction

Golafsoun Ameri, Victor Yang, Carl Kumaradas

Ryerson University, Department of Physics, Toronto, Ontario, Canada, M5B 2K3

E-mail: gameri@ryerson.ca

***Introduction*:** Acoustic microscopy (AM) refers to ultrasound imaging performed at frequencies above 100 MHz. Images with lateral resolutions of up to 3 μm can be obtained in acoustic microscopy. The applications of this imaging technique in cell death monitoring and evaluation of cancer treatment effectiveness are being investigated with promising results. Acoustic microscopy uses a fixed element transducer with a tight focus. As a result, the imaging depth of field is limited to around 35.7 μm at 400 MHz. Array transducers, which can create dynamic focusing throughout the field of view, cannot be manufactured at such high frequencies with available technologies. One possible method that could be used to improve the image lateral resolution in acoustic microscopy in the areas outside of the focal region is the synthetic aperture (SA) reconstruction technique. SA algorithms utilize a single element transducer to mathematically synthesize the effect of a larger aperture and to make dynamic focusing and depth independent resolution possible. One of the SA imaging algorithms, referred to as synthetic aperture focusing technique (SAFT), was implemented in both time and frequency domain to reconstruct images of

simulated and experimental radio frequency (RF) data of a SASAM acoustic microscope (Kibero GmbH, St. Ingbert, Germany) at 400 MHz. In the implemented algorithms, the focus of the transducer was treated as a virtual point source producing diverging waves in all directions.

***Materials and Methods*:** The performance of SAFT in acoustic microscopy was investigated using both simulated and experimentally obtained data. FIELD II (J. A. Jensen, Technical University of Denmark) was used to simulate the acoustic field of the SASAM transducer and to calculate the backscattered echoes from point scatterers placed at different depths before and after the focus. Attenuation was included in the simulations and a 10 dB noise level was added to the simulated data. Experimental RF data of a micro-particle was obtained when placed at different distances with respect to the focus of the transducer. Moreover, the backscattered RF data of two micro-particles positioned closely to each other was acquired. Wiener filtering was applied to the simulated and experimental RF data before processing and apodization was included in the time domain SAFT algorithm to reduce the sidelobes.

***Results and Discussion*:** The tight focusing of the acoustic microscope makes it suitable for synthetic aperture imaging with a virtual source. A comparison of the reconstructed SAFT and conventional B-mode images showed a significant improvement of the lateral resolution in the images reconstructed with the SAFT algorithm in regions outside the focus. In one set of the experimental data, two micro-particles that could not be distinguished from each other in a conventional B-mode image were shown as separate entities in the SAFT reconstructed images. The lateral resolution of SA images without apodization were slightly superior to those obtained with apodization, while the sidelobe levels were lowered and visualization of the scatterers were improved in the case when apodization was utilized. The Wiener filter was effective in reducing the additive noise level in the images. While both time and frequency domain SAFT improved the image resolution, the frequency domain SAFT performed better than the time domain algorithm**.** SA imaging may improve cell image quality in AM, which has applications in treatment monitoring.

Key words: Synthetic aperture imaging; Acoustic microscopy; Lateral resolution; Apodization.

Microbubbles Enhance Therapeutic Effect of HIFU: Effect of Exposure Conditions on Thermal Lesion Volume and Temperature

Sonal Bhadane, Jahan Tavakkoli, Raffi Karshafian

Ryerson University, Department of Physics, Toronto, Ontario, Canada, M5B 2K3

E-mail: sbhadane@ryerson.ca; karshafian@ryerson.ca

***Introduction*:** High-intensity focused ultrasound (HIFU) is used to ablate a preselected solid tumor volume within the body without harming the overlying tissues by converting ultrasound energy into heat. Currently, limitations associated with HIFU tumor ablation include the long treatment duration for large tumors and the reduced heat in highly vascularized tissue. This project aims to overcome limitations of HIFU using microbubble agents. Specifically, this study investigates the effects of microbubbles with HIFU on temperature rise and lesion formation in an *ex vivo* tissue model.

***Materials and Methods*:** *Ex vivo* tissue was treated with HIFU (2-MHz frequency) in absence and presence of microbubbles. A volume of 0.2 ml Artenga® microbubbles (concentration of around 10^9 microbubbles/ml, mean bubble diameter of 2-4 microns) was injected at the HIFU focus prior to ultrasound treatment. The temperature was measured using K type thermocouple. Following HIFU, tissue was sectioned and the coagulated lesion size was measured using a ruler. Lesion volume was estimated using the ellipsoid volume. Experiments were conducted at varying ultrasound intensities (600 to 2500 W/cm^2), microbubble concentrations (0 to 100%, 0.2 ml microbubble concentration) and exposure durations (3 to 10 seconds).

***Results and Discussion*:** The presence of microbubbles increased lesion volume and peak temperature induced with HIFU treatment. At intensity of 2316 W/cm^2, the lesion volume increased by ~2 folds – from 151.8 mm^3 to 323.21 mm^3 – and the peak temperature increased from 83.20°C to 99.43°C in the absence and presence (100% volume concentration) of microbubbles, respectively. These effects depended on microbubble concentration and ultrasound intensity. Lesions of comparable volumes were achieved at lower intensities and higher microbubble concentrations compared to higher intensities and lower microbubble concentration. The intensity required for producing tissue lesion decreased as microbubble concentration increased. For example, exposure at intensity of 2316 W/cm^2 and 50% of the microbubble concentration produced a lesion volume of 220 mm^3. Whereas at 100%

microbubble concentration, a similar lesion volume required an intensity of 1900 W/cm^2. The peak temperature increased as microbubble concentration increased from 83.20°C, 93.40°C and 99.43°C for 0%, 50% and 100% microbubble concentration, respectively. At lower intensities, there was no significant increase in the lesion volume, regardless of the microbubble concentration. For example at intensity 649 W/cm^2, the lesion volume increased from 3.84 mm^3 to 5.85 mm^3 for 0% to 100% microbubble concentrations. Comparing all insonations with the same exposure intensity, the duration required for producing tissue damage decreased as microbubble concentration increased from 0% to 100%. For example, at intensity of 2316 W/cm^2, 152.28 mm^3 lesion volume was produced at 5 s exposure time without microbubbles. Similar volume can also be produced with 100% microbubble concentration with 3 s exposure time.

The results indicate that the presence of microbubbles in tissue increase the tissue ablation with reduced intensity and duration. This study suggests that with proper optimization of the HIFU exposure and microbubble concentration, greater treatment efficiency can be achieved which may lead to reduction in the total treatment duration and intensity.

Key words: High intensity focused ultrasound; Microbubbles.

An Individualized Dose/Schedule Strategy for Sunitinib in Metastatic Renal Cell Cancer (mRCC) May Improve Progression Free Survival (PFS): Correlation with Dynamic Microbubble Ultrasound (DCE-US) Data

G. A. Bjarnason[1], B. Khalil[1], R. Williams[2], J. M. Hudson[2], B. Lloyd[2], L. M. Milot[3], M. Atri[4], A. Kiss[5], P. Burns[2]

[1]Sunnybrook Odette Cancer Centre, Toronto, ON, Canada, M4N 3M5

[2]Imaging Research, Sunnybrook Health Sciences Centre, Toronto, ON, Canada, M4N 3M5

[3]Medical Imaging, Sunnybrook Health Sciences Centre, Toronto, ON, Canada, M4N 3M5

[4]Joint Department of Medical Imaging, University of Toronto Health Network, Toronto, ON, Canada, M5G 2C4

[5]Department of Research Design and Biostatistics, Sunnybrook Health Sciences Centre, Ontario, Canada, M4N 3M5

E-mail: georg.bjarnason@sri.utoronto.ca

***Introduction*:** Sunitinib area under the curve (AUC) correlates with response and PFS (Houk *et al*.). Current recommendations for dose/schedule modification do not take this into account.

***Materials and Methods*:** A single center retrospective review identified mRCC patients (pts) where individualized (individ.) sunitinib dose/schedule modifications (DSM) were used to maximize dose and minimize time off therapy (Rx). Pts were started on 50 mg 28 days (d) on/14 d off. DSM were done to keep toxicity (hematology, fatigue, skin, GI) at ≤grade-2. DSM-1 was 50 mg 14 d/7 d with individ increases in d on Rx based on toxicity. DSM-2 was 50 mg 7 d/7 d with individ increases in d on Rx. DSM-3 was 37.5 mg continuously with individ 7 d breaks. DSM-4 was 25 mg continuously with individ 7 d breaks.

***Results*:** In 172 pts; median age was 60 y; 20% good, 60% intermediate, 20% poor prognosis by Heng criteria; 80% had nephrectomy; 79% clear cell histology; 60% were previously untreated. At a median follow-up of 14.3 months (mo), overall median PFS was 8.9 mo. Pts were allocated to three groups based on the dose/schedule used for the longest time. The

PFS/Response (PR+SD) for each group was 4.9 mo/64.1% (standard 50 mg 28 d/14 d; 39 pts), 11.5 mo/77.5% (DSM-1/DSM-2; 71 pts) and 11.9 mo/82.3% (DSM-3/DSM-4; 62 pts) with improved PFS ($p = 0.0001$) and higher response (ns) in both DSM groups vs. the standard schedule. In a subgroup of 103 clear cell cancer pts the PFS/response for each group was 5.8 mo/73.7% (standard 50 mg 28 d/14 d; 19 pts), 14.9 mo/83.7% (DSM-1/DSM-2; 43 pts) and 14.7 mo/82.9% (DSM-3/DSM-4; 41 pts) with improved PFS ($p = 0.001$) and higher response in both DSM groups vs. the standard schedule. The PFS in the DSM groups is similar in the 172 unselected pts, and better in the 103 clear cell pts, than in the Sunitinib pivotal trial (PFS 11 mo). All 13 pts still on therapy are on a DSM Rx. In 12 responding pts studied by DCE-US at baseline, and after 7 d and 14 d on Rx or after 14 d and 28 d on Rx, tumor blood volume decreased at d 7 and again at d 14 vs. baseline but was stable or increased at d 28 vs. d 14. A rebound was seen after 14 d off Rx. The majority (67%) of the response to sunitinib treatment occurs in small vessels characterized by slow flow velocities by DCE-US. Sunitinib PK data from 23 imaged pts, correlate inversely with blood volume and blood flow velocity data on DCE-US.

***Discussion*:** DCE-US would have predicted that a 14 d/7 d was better than a 28 d/14 d schedule for Sunitinib. DCE-US is as a surrogate marker for pharmacodynamics of antiangiogenic drugs and can help predict the best dose and schedule for novel agent. This DSM strategy was associated with a favorable toxicity profile, apparent improvement in PFS and a good PR+SD rate. Starting pts on 50 mg 14 d/7 d followed by individ DSM is be safe and active. Pts that tolerate 50 mg 28 d/14 d with minimum toxicity need dose escalation and/or less time off therapy to optimize PFS. A prospective confirmatory study is planned.

Key words: Kidney cancer; Sunitinib; Microbubble; Ultrasound.

Ultrasound Shear Wave Induced Resonance Elastography of Breast Lesions with Polarized Torsional Waves

Anis Hadj Henni[1], Cédric Schmitt[1,2], Didace Ekeom[1], Isabelle Trop[3,4], Guy Cloutier[1,2,4]

[1]Laboratory of Biorheology and Medical Ultrasonics, University of Montreal Hospital Research Center (CRCHUM), Montreal, QC, Canada, H2L 2W5

[2]Institute of Biomedical Engineering, University of Montreal, Montreal, QC, Canada, H3C 3J7

[3]Department of Radiology, University of Montreal Hospital (CHUM), Montreal, QC, Canada, H2L 4M1

[4]Department of Radiology, Radio-Oncology and Nuclear Medicine, University of Montreal, Montreal, QC, Canada, H3T 1J4

E-mail: guy.cloutier@umontreal.ca

***Introduction*:** Shear Wave Induced Resonance (SWIR) is a new technique for dynamic ultrasound elastography of confined mechanical inclusions. It relies on the polarization of shear waves to induce the mechanical resonance of the inclusion. By properly identifying the resonance spectrum and with *a priori* knowledge on the lesion dimension, its viscoelasticity can be retrieved with an inverse problem formulation. A generalization of SWIR elastography for breast tumour imaging is proposed. This study is addressing the forward problem formulation (*i.e.*, the theoretical modeling and experimental validation of propagating shear waves to induce resonance).

***Materials and Methods*:** A theoretical model based on the Helmholtz equation in spherical coordinates was implemented to simulate and understand the mechanism of resonance of spheres by torsional waves. *In vitro* phantom experiments were also conducted to demonstrate the possibility of polarizing torsional waves to induce the mechanical resonance of a soft inclusion. The experimental set-up was also adapted to prove the feasibility of inducing resonance of an *in vivo* breast fibroadenoma.

***Results and Discussion*:** The theoretical model and *in vitro* experimental set-up allowed imaging the three first eigenfrequencies and eigenmodes of a soft sphere. Experimental displacement maps at resonance were correlated with theory permitting the validation of the model. The preliminary *in vivo* SWIR measurement on the breast fibroadenoma is presented in Figure 1. Despite current technical limitations

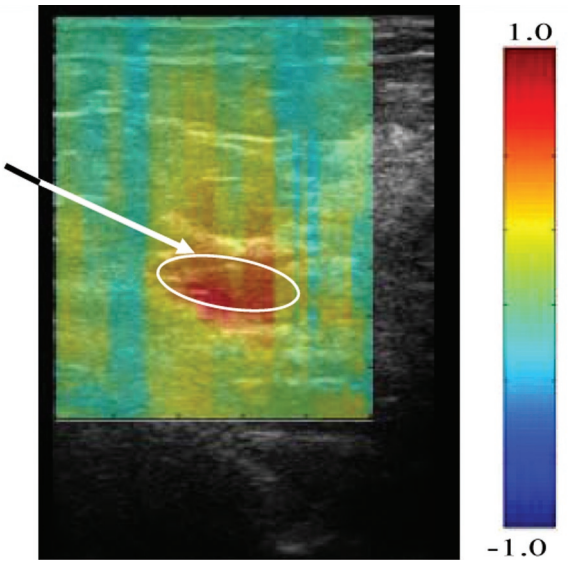

Figure 1: Ultrasound B-mode image of a 11-mm by 5-mm fibroadenoma (white ellipse) in the left breast of a 44 year old women with superposition on the B-mode image of the normalized stationary displacement map corresponding to the resonance frequency of the lesion of 80 Hz.

of the implemented technique for *in vivo* validation, results revealed the potential of SWIR elastography to segment and mechanically characterize breast lesions. The design of an octagonal ultrasound probe for breast cancer screening and diagnosis is finally proposed to optimize future developments on SWIR breast imaging.

Key words: Ultrasound imaging; Dynamic shear wave elasticity imaging; Breast imaging; Viscoelasticity.

Quantification of Microvascular Response to Radiation Therapy Using Optical Coherence Tomography

Leigh Conroy[1], Azusa Maeda[1], John G. Sled[1,2], Ralph S. DaCosta[1,3,4], I. Alex Vitkin[1,3,4]

[1]Department of Medical Biophysics, University of Toronto, Toronto, ON, Canada

[2]Mouse Imaging Centre, Hospital for Sick for Sick Children, University of Toronto, Toronto, ON, Canada

[3]Ontario Cancer Institute, University Health Network, Toronto, ON, Canada

[4]Radiation Medicine Program, University of Toronto, Toronto, Ontario, Canada

E-mail: leigh.conroy@utoronto.ca

***Introduction*:** Over half of all cancer patients receive radiation therapy (RT) as part of their treatment (1). Ionizing radiation has been thought to be curative by directly killing tumor cells and by damaging their genetic material (DNA); however, recently the tumour vasculature has become recognized as a critical regulator of biological response of tumours to ionizing radiation (1). Despite this clinical relevance, these effects are poorly understood and are rarely used in radiation treatment planning and monitoring. Here we demonstrate the use of speckle-variance optical coherence tomography (OCT) to monitor the *in vivo* radiobiological response of tumor vasculature to radiation therapy, and the development of specific metrics to quantitatively evaluate the longitudinal effect of radiation therapy on tumor vascular networks.

***Materials and Methods*:** A dorsal skin-fold window chamber (WC) was implanted in female nude mice to provide direct visualization of tumour (ME180 human cervical cancer) microvasculature and microstructure *in vivo*. A small animal x-ray micro-irradiation system was used to deliver 30-Gy single dose focal irradiation to tumours within the WC. Speckle-variance optical coherence tomography (svOCT) was used to longitudinally image tumours over 18 days as to monitor radiation-induced changes in microvasculature. A 3D skeletonization algorithm was applied to svOCT images and metrics such as number of vessels, vessel length, branch points and tortuosity were extracted. A 3D vessel tracking algorithm is also being optimized for the extraction of additional metrics such as vessel diameter, location and connectivity.

***Results and Discussion*:** The svOCT system provided high resolution (~10 μm) images of microvasculature for moni-

toring dynamic tumour radiobiological response *in vivo*. Speckle-variance images enabled qualitative observation of vascular shut-down, remodeling and reperfusion following irradiation. Metrics indicative of vessel structure and function were derived, for example the number of vessels inside the tumour as a metric to monitor radiation damage and radiation-induced angiogenesis; tortuosity as an indicator of vessel function and transport, and fractal dimension to describe organization and self-similarity in vascular networks. Preliminary results indicate that the developed metrics can be used to monitor vascular response to radiation therapy and give insight into underlying radiobiological vascular changes.

Key words: Radiation therapy; Optical coherence tomography; Optical imaging; Tumor vasculature.

1. Garcia-Barros, M., Paris, F., Cordon-Cardo, C., Lyden, D., Rafii, S., Haimovitz-Friedman, A., *et al.* Tumor response to radiotherapy regulated by endothelial cell apoptosis. *Science*, May 16, *300*(5622): 1155-9 (2003).

Hyperpolarized Mri Methods for Therapy Monitoring

Charles H. Cunningham[1,2]

[1]Imaging Research, Sunnybrook Health Sciences Centre, Toronto, ON, Canada

[2]Department of Medical Biophysics, University of Toronto, Toronto, ON, Canada

E-mail: chuck@sri.utoronto.ca

***Introduction*:** Metabolism in primary and metastatic cancers is abnormal. As a result of nearly 100 years of studies, we now understand that multiple metabolic pathways may be disrupted and that in untreated cancers, oncogenes control the expression of the individual enzymes that regulate cancer metabolism. After treatment, the overall metabolic profile reflects the interactions of cancer genetics with the direct and indirect effects of therapy. A long-standing goal of imaging technologies such as positron tomography and magnetic resonance imaging has been to monitor these abnormal pathways in patients.

Physicists have known for many years that the sensitivity of magnetic resonance can be improved by a factor of 10,000-100,000 through redistributing the populations of nuclear spins in a magnetic field, a process termed "hyperpolarization". Only recently was it appreciated that imaging hyperpolarized nuclei and their metabolic products is feasible *in vivo*.

***Methods*:** Transfer of this technique to the clinic may allow an oncologist to determine whether a cancer is responding to the treatment within hours of treatment. If the tumor is not responding, a more effective treatment regime could be initiated; rapidly changing the patient to a more effective drug is not only cost-effective but can also greatly improve morbidity and mortality.

***Results*:** Figure 1.

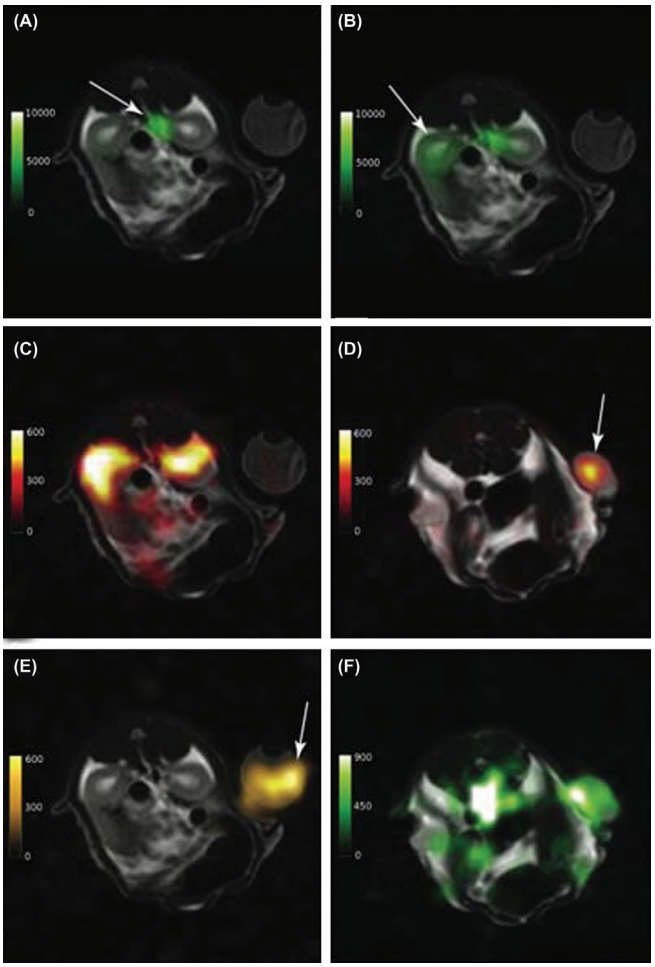

Figure 1: Example ^{13}C imaging data from a rat model of cancer. (**A**) The time-frame 5 s after the start of the injection shows pyruvate (green color-map) confined within the descending aorta (arrow), on its way to downstream tissues. (**B**) The next time-frame (10 s after the start of injection) shows [1-^{13}C] pyruvate within the kidneys. Note the excellent correspondence between ^{13}C signal and anatomical detail in the T2-weighted images, particularly the pyruvate in the aorta. (**C**) Lactate (orange color-map) within the kidneys and (**D**) within the implanted tumor can be observed at this same time-point. (**E**) The signal from the thermally polarized [1-^{13}C] urea reference phantom is shown, as well as (**F**) the [1-^{13}C] pyruvate signal from the same time frame as (**D**).

Key words: Hyperpolarization; Pyruvate; Metabolism.

1. Ardenkjaer-Larson, J. H., *et al.* Increase in signal-to-noise ration of >10,000 times in liquid-state NMR. *Proc Natl Acad Sci U S A 100*, 10158-10163 (2003).

2. Day, S. E., Kettunen, M. I., *et al.* Detecting tumor response to treatment using hyperpolarized ^{13}C magnetic resonance imaging and spectroscopy. *Nature Medicine 13*, 1382-1387 (2007).

Novel Conventional Frequency Detection of Cell Death *In Vivo* with Neoadjuvant Chemotherapy for Locally Advanced Breast Cancer

Czarnota G. J.[1,2], Lee J.[2], Papanicolau N.[2], Sofroni E.[1], Iradji S.[1], Kolios M. C.[3]

[1]Imaging Research and Radiation Oncology, Sunnybrook Health Sciences Centre, Toronto, ON, Canada, M4N 3M5

[2]Departments of Radiation Oncology and Medical Biophysics, University of Toronto, Toronto, ON, Canada, M4N 3M5

[3]Ryerson University, Department of Physics, Toronto, Ontario, Canada, M5B 2K3

E-mail: gregory.czarnota@sunnybrook.ca

***Introduction*:** We have previously demonstrated that high-frequency ultrasound and spectral analysis can detect cell death. Here we investigate whether conventional frequency (7 MHz) ultrasound incorporating spectral analysis may be used for the same purpose *in vivo* in human patients receiving chemotherapy.

***Materials and Methods*:** A clinical study was undertaken investigating the efficacy of ultrasound to quantify cell death in tumor responses with cancer treatment. Patients (n = 60) with locally advanced breast cancer received anthracyline and taxane-based chemotherapy treatments. Data collection consisted of acquiring tumor images and radiofrequency data prior to treatment onset and at 4 times during treatment (weeks 0, 1, 4, 8 and preoperatively). Digital low-frequency ultrasound data was sampled with an 15-bit dynamic range using an Ultrasonix-RP device with a 7 MHz central frequency (3-10 MHz –6 dB range). Whole mount histology was obtained for all samples.

***Results and Discussion*:** Data indicate increases of approximately 9 dBr (+/− 1.67) in ultrasound backscatter in patients who responded to treatment. Patients assessed as responding poorly demonstrated significantly lower increases (2.3 +/− 1.7 dBr). Increases in 0-MHz intercept followed similar trends while increases in spectral slope were observed from tumor regions demonstrating increases in tissue echogenicity.

***Conclusions*:** This study demonstrates the potential of ultrasound to quantify changes in tumours in response to cancer treatment administration in a clinical setting. This approach may assist in the customization of cancer treatments facilitating switching from ineffective treatments to efficacious therapies.

Thermal Dose Based Monitoring of Thermal Therapy for Prostate Cancer

David Dalla Rosa, J. Carl Kumaradas

Ryerson University, Department of Physics, Toronto, Ontario, Canada, M5B 2K3

E-mail: david.dallarosa@ryerson.ca

***Introduction*:** Thermal therapy is an ever-growing field of treatment in medicine. Coagulative thermal therapy utilizes heat alone to destroy the targeted area. When temperatures rise above 60°C, tissue proteins denature resulting in coagulative necrosis (cell death). Thermal dose models are used to predict the amount of damage from heating a target for a certain length of time. The current model, which provides a "cumulative equivalent minutes at 43°C" (CEM43) metric, has been found to be inaccurate at the high temperatures used in coagulative thermal therapy. A new dose model, known as the "improved cumulative equivalent minutes at 43°C" (iCEM43), has been recently introduced and is being tested using clinical data of patients undergoing laser interstitial thermal therapy (LITT) to treat prostate cancer.

***Materials and Methods*:** Three dimensional patient-specific magnetic resonance (MR) imaging data has been acquired for a number of different patients with varying heating locations, number of heating locations, and size of region to be treated. Each set of patient data consists of full MR thermometry (MRTI) maps for each thermal lesion, taken every 6 seconds, as well as post-treatment gadolinium contrast enhanced MRIs (Gd-MR), and the contours corresponding to the region of perfusion shutdown delineated by a radiologist.

First, the contrast enhanced MRI and the temperature maps were co-registered accounting for both magnification and translation. For each temperature map, the thermal dose was then calculated using both the CEM43 and iCEM43 thermal dose models. The damage coordinates were then used to create a binary image representing the region of damage based on the Gd-MR contours. Using the calculated thermal dose maps, the threshold dose for each slice that best matched the region in the binary image was found for both the CEM43

and iCEM43 models, based on the dice similarity coefficient (DSC). In theory, since the same endpoint (perfusion shutdown) is being used in all cases, the threshold dose values should be very similar, if not equal (ideal case).

***Results and Discussion*:** The most complete analysis at the present moment is that of patient 9, which was a single heating location with 5 MR thermometry maps each one separated by 3 mm. The first noticeable result is that the iCEM43 threshold doses (minutes at 43°C) were all smaller ranging from 1.28×10^4 minutes to 3.59×10^4 minutes, compared to the CEM43 values ranging from 7.29×10^4 to 1.82×10^6. As can be seen, this leaves the iCEM43 model with an average threshold dose of $1.92 \times 10^4 \pm 1.04 \times 10^4$ minutes as compared to the CEM43 average dose value of $4.53 \times 10^5 \pm 7.63 \times 10^5$ minutes. These results indicate that the iCEM43 is more consistent in predicting perfusion shutdown in the LITT prostate treatment being investigated. The improved dose model will provide the ability to monitor real-time damage accumulation during thermal therapy using MRTI with more accuracy than the currently used model.

***Acknowledgements*:** The authors are grateful to both Dr. John Trachtenburg for releasing the patient data and Mr. Sean Davidson for technical assistance in interpreting the data.

Key words: Thermal dose; Thermal therapy; Prostate cancer; MR Thermometry.

Mechanisms in Ultrasound Enhanced Delivery

Cheri X. Deng

Department of Biomedical Engineering, University of Michigan, Ann Arbor, MI 48105, USA

E-mail: cxdeng@umich.edu

***Introduction*:** Microbubble-facilitated sonoporation, or the ultrasound-induced disruption of the cell membrane, provides new opportunities for non-viral delivery of therapeutic agents into viable cells. However, sonoporation has relatively low delivery efficiency and often variable outcome. The detailed processes of sonoporation and the ensuing intracellular transport have not been completely understood and quantified, particularly at the single cell level. Precise control of cavitation and real-time assessment of the ensuing sonoporation in a spatiotemporally correlated fashion have been one of the major difficulties in the mechanistic study of sonoporation. The goal of our study is to gain understanding of the mechanisms of sonoporation in order to develop rational approaches to improve sonoporation delivery.

***Materials and Methods*:** *In vitro* studies were conducted using several types of cells, either adherent, or suspension, or in 3D spheriods. Ultrasound application was performed with 1.25 MHz single element ultrasound transducer driven by signal generators and power amplifiers. Preformed non-targeted and targeted microbubbles that can be attached to the cell membrane were used. Optical/acoustic techniques were also employed to control the microbubble locations and cavitation. Voltage clamp/patch clamp recordings were used to monitor the changes of cell membrane permeability in real time in sonoporation. Multi-wavelength fluorescence microscopy was used to image changes of intracellular calcium concentration, intracellular transport, as well as gene transfection. High-speed bright field imaging was synchronized with ultrasound exposures and other measurements to capture microbubble excitation driven by ultrasound pulses.

***Results and Discussion*:** This study developed an integrated and interdisciplinary approach that combines optical, ultrasonic, and electrophysiology techniques to control ultrasound-driven microbubble cavitation and activities and measure the resulting change of cell membrane permeability in real-time at the single cell level. Using this method, quantitative correlation of ultrasound-driven microbubble activities and sonoporation was obtained. Detail processes of pore formation and resealing affected by ultrasound and chemical factors were obtained. These results provide important, sometimes intriguing details, about sonoporation-mediated drug delivery and gene transfection that need to be considered for development of the technique for future translation applications for cancer treatment and diseases.

Key words: Sonoporation; Ultrasound; Microbubbles; Intracellular delivery; Membrane permeability.

High-Frequency 3D Power Doppler for Assessing Tumor Blood Vessel Response to Vascular Targeting Strategies

Ahmed El Kaffas[1,2], Sheldon Kwok[1,2], Anoja Giles[1,2], Gregory J. Czarnota[1,2]

[1]Imaging Research and Radiation Oncology, Sunnybrook Health Sciences Centre, Toronto, ON, Canada

[2]Departments of Radiation Oncology and Medical Biophysics, University of Toronto, Toronto, ON, Canada

E-mail: aelkaffas@gmail.com

***Introduction*:** High-frequency power Doppler ultrasound is a non-invasive vascular imaging modality ideal for quantitative assessment of vascularity in preclinical tumour models. With recent interest in strategically combining vascular targeting agents with radiation therapy to enhance tumor response, power Doppler offers a potent solution to assess the effects of such therapies. Our aim was thus to investigate the role of blood vessels in radiation response and how blood vessels can be targeted to enhance treatments using high-frequency power Doppler ultrasound.

***Materials and Methods*:** Breast cancer MDA-MB-231 xenografts were treated with single radiation doses of 0 to 16 Gy alone, or in combination with Sutent, an anti-angiogenic agent. Three-dimensional ultrasound tumour data were acquired before and 24 hours after treatment using a 25 MHz transducer and a VEVO770. The vascularity index (VI) was used to quantify blood from power Doppler data, while quantitative ultrasound spectroscopy (QUS) was used to monitor tumor cell death. Staining using TUNEL and CD31 of tumor sections was used to measure cell death and tumour vasculature distributions.

***Results and Discussion*:** Results indicated a VI decrease of up to 50% when tumours were irradiated with 8 and 16 Gy. Sutent and radiation combination treatments showed an increase in the VI, which may be associated with a vascular normalization effect. Analyses with QUS and TUNEL staining indicate an enhanced dose-dependent increase in tumor cell death when radiation was combined with Sutent. These results suggest that Sutent treatment may radiosensitize tumors by altering the tumor microenvironment.

Key words: Power doppler; Tumor vasculature; Radiation; Vascularity index (VI); Antiangiogenic.

Improved Objective Selection of Power Doppler Wall Filter Cut-Off Velocity for Accurate Vascular Quantification

Mai Elfarnawany[1,3,4], Stephen Z. Pinter[1,3]*, James C. Lacefield[1,2,3,4]

[1]Biomedical Engineering Graduate Program, Department of Radiology, University of Michigan, Ann Arbor, MI

[2]Departments of Electrical & Computer Engineering and Medical Biophysics, University of Western Ontario, London, Ontario, Canada

[3]Robarts Research Institute, Department of Radiology, University of Michigan, Ann Arbor, MI

[4]Biomedical Imaging Research Centre, University of Western Ontario, London, Ontario, Canada

E-mail: melfarna@imaging.robarts.ca

***Introduction*:** User settings of power Doppler acquisition parameters such as the wall filter cut-off velocity have a significant impact on the amount and nature of artifacts in an image and can reduce the accuracy of vascular quantification in preclinical angiogenesis studies using high-frequency power Doppler. We developed the wall filter selection curve (WFSC) method (1, 2) to objectively select the cutoff velocity that minimizes these artifacts and, hence, improves vascular quantification. A WFSC is constructed by plotting the colour pixel density (CPD) as a function of the cut-off velocity and is characterized by the presence of one or more characteristic intervals. Characteristic intervals are hypothesized to identify the cut-off velocity at which the CPD best estimates the vascular volume fraction of the imaged vessels. This paper presents a redesigned WFSC method that improves its automation and accuracy.

***Materials and Methods*:** The method is applied to subregions within the Doppler image to adapt the cutoff velocity to local variations in blood flow. Characteristic intervals in each subregion are automatically detected by applying a customized *N*-point maximum envelope peak detection algorithm (3) to the first difference of the CPD data. An operating point cut-off velocity is automatically selected at either the right end or the middle of the detected interval based on the slope of the interval relative to the remaining portions of the selection curve as well as the slopes of intervals in the surrounding subregions. Images are reconstructed using potentially different cut-off velocities in each subregion. The performance of the redesigned method was evaluated in 30-MHz power Doppler images of a four-vessel flow phantom.

***Results and Discussion*:** Characteristic intervals identified by the redesigned algorithm consistently enclosed intervals of minimum variation in CPD and agree with intervals found by visual inspection. For more than 70% of the analyzed subregions, the selected operating point corresponded to the CPD closest to the reference vascular volume fraction of the phantom. The redesigned method improved vessel delineation in flow-phantom images compared to the original method. The CPD of the reconstructed images was within 3% of the reference vascular volume fraction. The improved automation and performance of the redesigned WFSC method enhances its suitability for online implementation in a power Doppler scanner, which should make power Doppler a more robust tool for quantifying responses to anti-vascular and anti-angiogenic therapies.

Key words: High-frequency ultrasound; Power doppler; Microvascular imaging; Vascular quantification.

1. Pinter, S. Z., Lacefield, J. C. *Ultrasound Med Biol 35*, pp. 1217-1228 (2009).
2. Pinter, S. Z., Lacefield, J. C. *IEEE Trans Med Imaging 29*, pp. 1124-1139 (2010).
3. Judd, M. D. *IEEE Trans Aerosp Electron Syst 28*, pp. 1158-1163 (1992).

Diffuse Optical Spectroscopy Evaluation of Treatment Response in Patients With Locally Advanced Breast Cancer Receiving Chemotherapy

Omar Falou[1,2], Hany Soliman[1,2], Sara Iradji[1], Jacqueline Spayne[1,2], Rebecca Dent[3], Martin Yaffe[1,2], Gregory J. Czarnota[1,2]

[1]Imaging Research and Radiation Oncology, Sunnybrook Health Sciences Centre, Toronto, ON, Canada, M4N 3M5

[2]Departments of Radiation Oncology and Medical Biophysics, University of Toronto, Toronto, ON, Canada, M5S 1A1

[3]Department of Medical Oncology, Sunnybrook Health Sciences Centre, Toronto, ON, Canada

E-mail: omar.falou@sunnybrook.ca

***Introduction*:** The necessity for a non-invasive and inexpensive imaging modality to both diagnose and monitor treatment response has lead to renewed interest in the potential of optical imaging. The aim of this study is to investigate the potential of diffuse optical spectroscopy (DOS) for monitoring of patients with locally advanced breast cancer (LABC) undergoing chemotherapy.

***Materials and Methods*:** Fifteen women receiving various neoadjuvant treatments for locally advanced breast cancer had the affected breast scanned 5 times: before, 1 week, 4 weeks, and 8 weeks following initiation of the treatment and prior to surgery. Three-dimensional maps of optical absorption and scattering properties of the tumour at different wavelengths (690 nm, 730 nm, 780 nm, and 830 nm) were obtained using the SoftScan commercial DOS system (ART Inc., Montreal, QC, Canada). Optical properties were converted to functional indices related to tissue microstructure and biochemical composition such as deoxygenated hemoglobin, oxygenated hemoglobin, total hemoglobin concentrations, water and lipid percentages, oxygen desaturation and saturation, scatter amplitude, scatter power and tissue optical index. Tumour response was evaluated from clinical and pathological responses using whole mount pathology after mastectomy. Comparisons between responders and non-responders were performed using a student *t*-test analysis (PASW Statistics 18, SPSS, Inc., Chicago, IL). Discriminant analysis was used to determine which optical parameters discriminate between responders and non-responders.

***Results and Discussion*:** Patients which responded to treatment showed an initial increase followed by a sharp decrease

in optical parameters measured in the whole breast compared to non-responders. Responding patients showed a significant increase of 117 ± 7%, 108 ± 8%, 110 ± 7%, 111 ± 11%, and 116 ± 15% in deoxygenated hemoglobin, oxygenated hemoglobin, total hemoglobin concentrations, water percentage, and tissue optical index, whereas non-responding patients showed a decrease of 86 ± 9%, 82 ± 7%, 83 ± 7% 71 ± 7%, and 68 ± 9% from baseline after the first week of the start of the treatment, respectively. Deoxygenated hemoglobin concentration and water percentage were found to be the best predictors of the treatment response. Results of this study suggest that optical parameters can be potentially used to predict and monitor patient's response to neoadjuvant chemotherapy.

Key words: Diffuse optical spectroscopy; Tissue spectroscopy; Neoadjuvant chemotherapy; Locally advanced breast cancer.

Detecting Apoptosis Using Optical Coherence Tomography Envelope Statistics, Spectral Parameters and Speckle Decorrelation

Golnaz Farhat[1,2], Adrian Mariampillai[3], Victor X. D. Yang[3], Michael C. Kolios[4], Gregory J. Czarnota[1,2]

[1]Imaging Research and Radiation Oncology, Sunnybrook Health Sciences Centre, Toronto, ON, Canada, M4N 3M5

[2]Departments of Radiation Oncology and Medical Biophysics, University of Toronto, Toronto, ON, Canada, M4N 3M5

[3]Department of Electrical and Computer Engineering, Ryerson University, Toronto, Ontario, Canada, M5B 2K3

[4]Department of Physics, Ryerson University, Toronto, Ontario, Canada, M5B 2K3

E-mail: golnaz.farhat@gmail.com

***Introduction*:** Apoptosis is a process by which a predictable sequence of biochemical and morphological changes leads to cell death. Morphologically, it is characterized by a rounding and shrinking of the cell, fragmentation of the nucleus and other organelles, membrane blebbing and, ultimately, disintegration of the cell into apoptotic bodies. We predict that the structural changes occuring as a result of cell death modify the optical properties of tissues, which can be probed using statistical and spectroscopic analysis of optical coherence tomography (OCT) data. We further hypothesize that the rate of intracellular motion in apoptotic cells will be higher than in viable cells due to cytoskeletal remodeling required for membrane blebbing and cell fragmentation, and predict that this increase in intracellular motion can be detected by measuring the speckle decorrelation rate in OCT images.

***Materials and Methods*:** Acute myeloid leukemia (AML) cells were treated with 10 µg/mL of cisplatin to induce apoptosis. Cell samples were imaged at 0 h, 2 h, 4 h, 6 h, 9 h, 12 h, 24 h and 48 h of cisplatin exposure. Prior to imaging treated cells were washed and centrifuged to create a tightly packed cell sample. Samples were subsequently fixed and processed for haematoxylin and eosin (H&E) staining. Data were acquired using a Thorlabs Inc. (Newton, NJ) swept source OCT system. Two-dimensional (2-D) data sets were collected in 10 separate planes within each sample. Statistical parameters were extracted from each data set by fitting a pixel intensity histogram to a generalized gamma (GG) probability distribution function. Normalized backscatter spectra were used to calculate the integrated backscatter (IB) and spectral slope (SS). Additionally, 10 series of 2-D data were recorded continuously over a period of 10 seconds at a frame rate of 166 Hz. From this data, intensity autocorrelation curves were calculated at each pixel location and an average decorrelation time was extracted.

***Results and Discussion*:** The IB increased by 2-fold over 48 hours with significant increases observed as early as 4 hours. The SS increased in steepness by 2.5-fold with significant changes at 12 hours, while the statistical parameters from the GG fits were sensitive to apoptotic changes at 24 to 48 hours. Histological analysis indicated nuclear condensation and fragmentation at 24 hours, suggesting the late scattering changes could be related to nuclear structure. Autocorrelations of OCT signal intensities acquired from acute myeloid leukemia cells as a function of treatment time demonstrated a significant drop in the decorrelation time after 24 hours of cisplatin treatment. This corresponded with nuclear fragmentation and irregular cell shape observed in histological sections which could be indicative of cell membrane blebbing.

Key words: Optical coherence tomography; Apoptosis; Spectroscopy; Envelope statistics; Speckle decorrelation.

Classification and Tissue-Type Imaging of Cancerous Prostate Tissue

Ernest J. Feleppa[1], Christopher R. Porter[2], Ronald Silverman[3]

[1]Lizzi Center for Biomedical Engineering, Riverside Research, New York, NY, USA

[2]Department of Urology, Virginia Mason Medical Center, Seattle, WA, USA

[3]Department of Ophthalmology, Columbia University Medical Center, New York, NY, USA

E-mail: efeleppa@riversideresearch.org

***Introduction*:** No reliable means of imaging prostate cancer currently exists. Therefore, biopsies are guided with respect to gross prostate anatomy and treatment involves the entire gland rather than being targeted to imaged lesions. A reliable means of imaging lesions could minimize false-negative biopsies, reduce the number of unwarranted biopsies, improve staging, direct treatment more effectively, reduce side effects, and provide a means of monitoring treated and untreated cancers. Tissue-type images (TTIs) based on spectrum analysis of ultrasonic echo signals and non-linear classification methods may provide the needed means of imaging the prostate.

***Materials and Methods*:** Radiofrequency ultrasonic echo signals were acquired and analyzed from 617 biopsied regions in 64 prostate patients. The examining urologist assigned a level-of-suspicion for cancer likelihood to each biopsy site based on conventional ultrasonic B-mode imaging combined with all available clinical information. Power spectra were computed from the acquired biopsy-region echo signals. Two spectral parameters characterizing the biopsied tissue were combined with PSA value and used to train and test two machine-learning tools for classification: artificial-neural-networks (ANN) and support-vector machines (SVMs). The gold standard for actual tissue type was the biopsy histology. A leave-one-patient-out approach was used to eliminate any bias caused by possible correlation of properties in test and training sets. Classifier performance was assessed using ROC methods. TTIs were generated from the two computed spectral-parameter values combined with PSA values using a lookup Table that translated parameter and clinical-variable values into a score for the relative likelihood of cancer at each pixel. The scores were expressed as gray-scale or false color at every pixel in a user-specified region of interest.

***Results and Discussion*:** ANN classification of prostate biopsy-region echo-signal data produced an area under the ROC curve (A_Z) of 0.84; SVM classification produced a virtually identical A_Z. In comparison, baseline ROC curves derived from level-of-suspicion values assigned to the biopsy site resulted in an A_Z of 0.64. The associated ROC curves presented a sensitivity improvement of more than 50% for the machine-learning classifiers compared to impressions based on conventional B-mode images and clinical information. Furthermore, TTIs using lookup Tables derived from these classifiers successfully depicted cancers that were not detected using conventional imaging methods. The spectrum-analysis methods underlying TTIs exploit information that is discarded in generating conventional ultrasound images. Combined with clinical variables such as PSA, parameters derived from acoustic-backscatter power spectra appear to have a strong potential for reliably distinguishing cancerous from non-cancerous prostate tissue when classified by modern machine-learning tools such as ANNs and SVMs. In a clinical context, the TTIs made possible by these tools may offer markedly improved means of guiding biopsies, staging disease, and planning, targeting, and monitoring therapy for prostate cancer.

Key words: Prostate cancer; Tissue-type images; Biopsy guidance; Staging; Treatment planning; Treatment targeting; Treatment monitoring; Artificial neural networks; Support-vector machines.

Perfluorocarbon Droplets as a Drug Delivery System

Mario L. Fabiilli, Oliver D. Kripfgans, Justin R. Rajian, Xueding D. Wang, Paul L. Carson, J. Brian Fowlkes

Department of Radiology, University of Michigan, Ann Arbor, MI, 48109-5667

E-mail: Fowlkes@umich.edu

***Introduction*:** The development of acoustic droplet vaporization (ADV) began with single emulsion formulations of perfluorocarbon that could be used to generate microbubbles. These emulsions are stabilized by external shells that inhibit coalescence of the droplets. More recently (1, 2), we have developed double emulsions that can stabilize both the perfluorocarbon that undergoes vaporization and an aqueous or non-aqueous phase to support delivery of drugs. In addition, we have examined the encapsulation of a photoacoustic (PA) contrast agent that could ultimately provide *in situ* monitoring of drug release (3).

***Materials and Methods*:** Droplets were formulated using a two-step process with perfluorocarbon, either perfluoropentane

or perfluorohexane, and either water or oil to form double emulsions. The resulting droplets were tested to determine the acoustic conditions required for triggering the release of oil- or water-soluble compounds encapsulated within the emulsion, including indocyanine green (ICG). The efficacy of the release was studied in terms of various endpoints including effects on solute retention with and without triggering, effects on cell cultures, and the PA signal changes with wavelength.

***Results and Discussion*:** Double emulsions were formed with both oil and water phases that would retain solutes for triggered release. Upon vaporization, up to an 8 fold increase in flux was observed for the released solute. Cellular growth inhibition was significantly increased following release by ADV of chlorambucil, a chemotherapeutic agent. The ratio of the PA signal intensities between 860 and 800 nm changed by up to 32% upon ADV-triggered release of ICG into canine blood. These results would indicate that ADV with double emulsions could provide a means for delivering lipophilic or hydrophilic payloads and a potential method for monitoring local drug release.

Key words: Drug delivery; Photoacoustics; Emulsions.

1. Fabiilli, M. L., Haworth, K. J., Sebastian, I. E., Kripfgans, O. D., Carson, P. L., Fowlkes, J. B., Delivery of chlorambucil using an acoustically-triggered perfluoropentane emulsion. *Ultrasound in Medicine and Biology 36*(8): 1364-1375 (2010).
2. Fabiilli, M. L., Lee, J. A., Kripfgans, O. D., Carson, P. L., Fowlkes, J. B., Delivery of water-soluble drugs using acoustically Triggered perfluorocarbon double emulsions. *Pharmaceutical Research 27*(12), 2753-2765 (2010).
3. Rajian, J. R., Fabiilli, M. L., Fowlkes, J. B., Carson, P. L., Wang, X. D. Drug delivery monitoring by photoacoustic tomography with an ICG encapsulated double emulsion. *Optics Express 19*(15), 14335-14347 (2011).

Ultrasound-Activated Microbubble Enhancement of Radiation Response of Tumor Xenografts: Investigation of Mechanism in *ASMase* +/+ and *ASMase* −/− Mice

Amr Hashim[1,2], Anoja Giles[1,2], Gregory J. Czarnota[1,2]

[1]Imaging Research and Radiation Oncology, Sunnybrook Health Sciences Centre, Toronto, ON, Canada, M4N 3M5

[2]Departments of Radiation Oncology and Medical Biophysics, University of Toronto, Toronto, ON, Canada, M4N 3M5

E-mail: amr.hashim@sunnybrook.ca

***Introduction*:** Studies have recently demonstrated that ultrasound-activated microbubbles may enhance tumor response to radiation due to the perturbing effect the treatment has on tumor vasculature. It was also observed *in vitro* that ceramide-mediated cell death occurs with microbubble and radiation treatment and that a differential effect takes places when the *acid sphingomyelinase* (*ASMase*) enzyme is inhibited. The *ASMase*-inhibited endothelial cells do not undergo apoptosis when treated allowing further angiogenesis to occur, causing tumor growth. The purpose of the study is to investigate the effect and mechanism of radiation combined with high-intensity focused ultrasound (HIFU) activated microbubbles on normal and *ASMase*-inhibited endothelial cells in *in vivo* tumor xenografts.

***Materials and Methods*:** A fibrosarcoma cell line (MCA-129) was injected in the right hind legs of wild type mice (C57BL/6) containing the gene for *sphingomyelinase* enzyme (*ASMase* +/+) and in genetically altered knock-out mice lacking the gene for the enzyme (−/−). Heterozygotes (+/−) were used as well, due to breeding limitations of the −/− and their survival limitations during experimentation. Animals for the experiment were divided into two cohorts, organized according to the type of mice mentioned above: *ASMase* +/+ and −/− or +/−. For each cohort, the Definity® (Lantheus Medical Imaging, Inc., North Billerica, MA, USA) microbubble concentrations and radiation dosage were varied to test tumour response under different treatment conditions. The microbubble concentrations investigated were 0%, 1% and 3%, and the radiation dosages, 0 Gy, 2 Gy and 8 Gy. These conditions were tested in all possible combinations over three different time intervals: 3 hours, 24 hours and 72 hours. In total, 27 conditions, with four mice (n = 4) per condition, were examined per cohort. Power Doppler images of tumors were collected for pre and

post treatment using a high-frequency transducer at 30 MHz (VEVO 770, VisualSonics, Toronto, ON, Canada).

***Results and Discussion*:** Through the analysis of the power Doppler images, we were able to quantify the change in tumor vasculature. Although the analysis is ongoing, very clear trends are already apparent through tabulation and graphical representations of the numerical quantification of the tumor vasculature. We observe, in *ASMase* +/+ mice, tumor vasculature decreases with radiation dosage increases. There is vasculature increase with no radiation (0 Gy), while there are higher rates of vasculature decrease with 2 Gy and 8 Gy, respectively. There is a further decrease in vasculature with increases in microbubble concentration. The greatest decrease in tumor vasculature for the 72-hour time interval is observed when the mice were treated with 3% microbubble concentration and 8 Gy radiation. However, a different trend is seen with the −/− mice. Particularly, an increase in tumor vasculature is observed after any treatment. Although a final quantification regarding the rates of increase with respect to the treatment has not yet been conducted, we see consistently that ultrasound-activated microbubble treatment enhances the diminishing of tumor vasculature in +/+ mice, while not having an effect in the decrease of tumor vasculature in the *ASMase* −/− mice.

Key words: Ultrasound (HIFU); Microbubble; Radiation; *Acid sphingomyelinase* (*ASMase*); Tumor.

Ultrasound-Enhanced Thrombolysis – Better Blood Clot Break-Up with Bubbles

Christy K. Holland[1], Jonathan T. Sutton[1], Stephen R. Perrin, Jr.[1], Kevin J. Haworth[1], Gail J. Pyne-Geithman[2]

[1]Internal Medicine, Division of Cardiovascular Diseases and Biomedical Engineering Program, University of Cincinnati, Cincinnati, OH, USA 45267-0586

[2]Department of Neurosurgery, University of Cincinnati, Cincinnati, OH, USA 45267-0517

E-mail: Christy.Holland@uc.edu

***Introduction*:** Ultrasound has been shown to increase rt-PA thrombolysis via stable cavitation, or sustained bubble activity, but this mechanism needs further optimization. Use of low-frequency ultrasound in combination with microbubbles stabilized against dissolution, in the form of ultrasound contrast agents, has resulted in greater lytic efficacy *in vitro*.

***Materials and Methods*:** The motivation for developing ultrasound-enhanced thrombolysis, and the existing evidence for its potential as an intervention for ischemic stroke, will be reviewed. Stable cavitation will be discussed and current *in vitro* and *ex vivo* studies of bubble-mediated rt-PA clot lysis will be summarized.

***Results and Discussion*:** Ultrasound-driven stable cavitation nucleated by an infusion of an echo contrast agent facilitates rt-PA thrombolysis. Optimization of this gently effervescent phenomenon has the potential to reduce the morbidity and mortality of victims of ischemic stroke.

Key words: Thrombolysis; Ultrasound-enhanced thrombolysis; Stable cavitation; Stroke therapy.

Contrast-Enhanced Ultrasound as a Biomarker of Anti-Angiogenic Response in Renal Cell Carcinoma

John M. Hudson[1,2], Ross Williams[1,2], Brendan Lloyd[1,2], Laurent Milot[2], Mostafa Atri[3], Georg Bjarnasson[4], Peter N. Burns[1,2]

[1]Department of Medical Biophysics, University of Toronto, Toronto, ON, Canada

[2]Sunnybrook Research Institute, Toronto, ON, Canada

[3]Joint Department of Medical Imaging/UHN, Toronto, ON, Canada

[4]Sunnybrook Odette Cancer Centre, Toronto, Ontario, Canada

E-mail: hudsonjm@gmail.com

***Introduction*:** Imaging strategies that monitor the response of cancers to vascular-targeted treatments are shifting from measurements that rely only on anatomical tumour size to protocols that include indicators of vascular physiology and function. This trend is in reaction to the growing evidence that the response of the tumour microcirculation to anti-angiogenic drugs occurs long before observable changes in tumour volume. Dynamic contrast enhanced ultrasound (DCE-US) is a promising modality that takes advantage of the unique properties of intra-vascular microbubble contrast agents to visualize and quantify the functional properties (*i.e.* blood volume and flow velocity) of the microcirculation.

***Materials and Methods*:** DCE-US employing the disruption-replenishment method measured the evolving tumour vascularity in 32 previously untreated patients with metastatic renal cell carcinoma throughout the first course of Sunitinib therapy (scans at day 0, 7, 14, 28 and 42). A perfusion model that accounts for the dynamics of microbubble contrast agents and the ultrasound field properties was applied to linearized time-intensity data sampled throughout the tumour mass. Parameters related to the tumour blood volume, mean flow velocity, and indices of vascular morphology were quantified during the treatment cycle.

***Results and Discussion*:** The magnitude of vascular response varied within the patient population. In general, blood volume decreased during the first two weeks of treatment (median change relative to baseline was −49% on day 7 and −76% on day 14), and rebounded two weeks after the treatment ended (median change was −54% relative to baseline on day 42) Figure 1. Once the relationship between clinical outcome and the responses observed with DCE-US are better understood, DCE-US methods may help to identify responsive patients, predict oncoming drug resistance, and individualize treatment protocols.

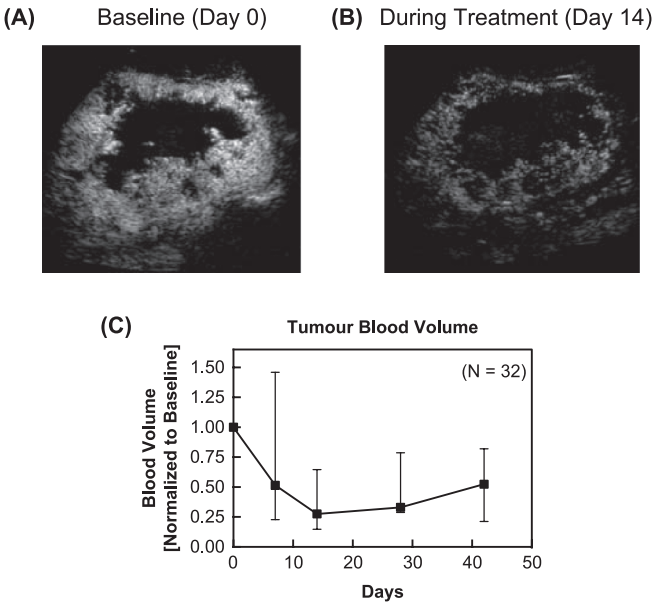

Figure 1: Contrast enhanced ultrasound images of a tumour (**A**) before and (**B**) 14 days into anti-angiogentic treatment. Anatomic size remains relatively constant while image intensity (related to blood perfusion) decreases. (**C**) In general, tumour blood volume decreases while on anti-angiogenic therapy and rebounds after treatment has stopped.

Key words: Dynamic contrast enhanced ultrasound; Microbubble contrast agents; Perfusion; Anti-angiogenic treatment; Renal cell carcinoma.

Photacoustic Spectral Analysis for Detecting Red Blood Cell Aggregation

Eno Hysi, Ratan K. Saha, Michael C. Kolios

Ryerson University, Department of Physics, Toronto, Ontario, Canada, M5B 2K3

E-mail: mkolios@ryerson.ca

***Introduction*:** The aggregation of red blood cells (RBCs) is a phenomenon governed by plasma fibrinogen concentration and the shear forces of flow. Increased RBC aggregation has been associated to a variety of pathological states such as diabetes and myocardial infarction. We propose the use of photoacoustics (PA) radiofrequency (RF) spectral analysis for the detection and characterization of RBC aggregation.

***Materials and Methods*:** A Monte Carlo based simulation was developed to differentiate aggregated (AG) and non-aggregated (NA) RBCs. It used a frequency-domain approach to calculate the PA pressure field generated by RBCs and then PA, RF spectral analysis to characterize the level of aggregation. The effect of hematocrit and aggregate size on the PA signals was investigated. Experimental confirmation of theoretical results was conducted using human RBC samples and the Imagio PA imaging device (Seno Medical Instruments Inc., San Antonio, TX). Aggregation was induced by suspending the RBCs in various concentrations of Dextran-70. To account for the response of the imaging system, the PA spectra were calibrated by dividing by the response of the transducer measured passively using a needle hydrophone. Spectral parameters such as the slope, intercept and midband fit are presented as a means for distinguishing between AG and NA samples.

***Results and Discussion*:** Theoretical and experimental results show a monotonic increase in the PA signal amplitude with increasing hematocrit. As the size of the aggregates increases, simulations demonstrate a shift towards lower frequencies in the PA power spectrum as well as enhancements as large as 11 dB compared to the NA sample. Experiments on AG samples demonstrate the ability of PA signals to detect changes in aggregation level controlled by Dextran-70 concentration. PA spectral parameters show enhancements as high as 5 dB (midband fit), 3.5 dB (intercept) and 0.3 dB/MHz (spectral slope) for AG RBCs compared to NA ones. It is important to note that the PA spectral parameters used here provide an accurate assessment of the changes that occur during the aggregation process. The PA technique discussed has never been applied to the detection and characterization of RBC aggregation and provides a quantitative mean for differentiating blood samples.

Key words: Photoacoustics; RBC aggregation; Tissue characterization.

Ultrasound and Microbubble Potentiated Enhancement of Chemotherapy *In Vitro*: Effect of Treatment Order and Acoustic Pressure

Firas Almasri, Raffi Karshafian

Ryerson University, Department of Physics, Toronto, Ontario, Canada, M5B 2K3

E-mail: karshafian@ryerson.ca; firas.almasri@ryerson.ca

***Introduction*:** Chemotherapy effectiveness depends on the ability of the drug molecules to penetrate tissues and cells, and to reach their intended target. It is limited by toxic side effects exerted by the therapeutic agent. The application of ultrasound and microbubbles has been shown to increase cell permeability and enhance intracellular delivery of cell-impermeable molecules, a process known as sonoporation. This work investigated the potential use of ultrasound and microbubbles to enhance the therapeutic effect of a chemotherapeutic agent using an *in vitro* cell suspension system. The objectives were to measure clonogenic cell viability following treatment with ultrasound and microbubbles in the presence and absence of a chemotherapeutic agent, treatment order, acoustic pressure and drug dose.

***Materials and Methods*:** Breast cancer (MDA-MB-231) cells in suspension were treated with ultrasound and microbubbles (USMB) at settings of 1 MHz pulse centre frequency, acoustic pressure (0, 0.5, 1.7 MPa peak negative pressure), 16 µs pulse duration, 1 kHz pulse repetition frequency, 60 s insonation time and 15 µl of Definity microbubbles in the presence and absence of chemotherapeutic agent docetaxel (Taxotere®). Cells were treated with docetaxel for five minutes and two hours. The order of USMB and chemotherapy (CM) were varied. Following treatment, cell viability was assessed using a clonogenic assay.

***Results*:** Cell viability was dependent on chemotherapy drug dosage and treatment duration; lower viability was achieved at higher chemotherapeutic concentrations and longer treatment durations as expected. Cell viability was ~44% at 0.01 nmol compared to ~83% at 0.0001 nmol CM dose for the 5 minutes treatment duration. Whereas, for the two hour CM treatment, cell viability was ~26% at 0.01 nmol compared to ~68% at 0.0001 nmol CM dose. Ultrasound microbubble treatment enhanced therapeutic effect of chemotherapy treatment. Cell viability decreased by ~5 folds with the combined treatment CM+USMB (~14%) compared to USMB treatment (~73%) at 1.7 MPa and CM alone (~65%) at 0.0001 nmol for two hour treatment. This effect depended on the chemotherapy treatment duration, ultrasound acoustic pressure, and treatment order. USMB treatment appears to have a more pronounced effect with longer CM treatment duration. The addition of USMB resulted in an additional 42% cell death (CM = 86% and CM+USMB = 44%) for 5 min treatment, whereas for the two-hour treatment, an additional 51% of cell death was achieved (CM = 65% and CM+USMB = 14%). Furthermore, lower viability was achieved with CM+USMB treatment order compared to USMB+CM. Cell viability of ~44% was achieved with the CM+USMB treatment order compared to cell viability of ~62% with the USMB+CM treatment order.

***Discussion and Conclusion*:** Ultrasound and microbubbles enhanced the therapeutic effect of docetaxel, a chemotherapeutic agent, with a more pronounced enhancement in the (CM+USMB) treatment order compared (USMB+CM) order. Cell death increased with increased drug dose and treatment duration. Future work will investigate this effect *in vivo*.

Key words: Microbubble; Sonoporation; Chemotherapy.

Single Cell Photoacoustics and More

Michael C. Kolios[2,3], Gregory J. Czarnota[1,2]

[1]Imaging Research and Radiation Oncology, Sunnybrook Health Sciences Centre, Toronto, ON, Canada, M4N 3M5

[2]Departments of Medical Biophysics, University of Toronto, Toronto, ON, Canada, M4N 3M5

[3]Ryerson University, Department of Physics, Toronto, Ontario, Canada, M5B 2K3

E-mail: mkolios@ryerson.ca

In ultrasound tissue characterization (UTC), the analysis of the frequency content of the radiofrequency (RF) backscattered signals provides information about tissue microstructure that typically cannot be resolved. New ultrasound instruments that allow easier access to the ultrasound RF data combined with more powerful computing platforms have enabled more research groups to explore the ideas related to tissue characterization, resulting in advances in the field. Examples include the characterization of the lymph nodes of cancer patients to find metastases, the differentiation of carcinomas and adenocarcinomas in mammary tumors and the use of these methods for treatment monitoring. In photoacoustic imaging, ultrasound waves are produced during the interaction or laser pulses with tissue chromophores. Just like

in ultrasound imaging, the radiofrequency (RF) signals are recorded to form an image, many times with the same commercial ultrasound scanners used in ultrasound imaging. The natural question arises: can the same ultrasound tissue characterization analysis techniques based on analysis of the RF data be adapted for photoacoustic imaging? If so, what is the interpretation of the data? It clearly would not be the same as in UTC, as the origin of the signal is not from the scattering of a propagating wave. In the presentation, several ideas as to the origin of the photoacoustic signals will be presented, as well as models that we have developed to understand how these signals can be interpreted. The answer may have its origins as that of the photoacoustic signal from a single cell.

Key words: Ultrasound tissue characterization; Photoacoustics.

Multi-Parametric MRI for Patient Selection in Focal Therapy of Prostate Cancer

Piotr Kozlowski[1,2,5], Silvia D. Chang[2], Edward J. Jones[3], Mehdi Moradi[4], S. Larry Goldenberg[5]

[1]UBC MRI Research Centre, Vancouver, BC, Canada
[2]Department of Radiology, University of British Columbia, Vancouver, BC, Canada
[3]Department of Pathology and Laboratory Medicine, University of British Columbia, Vancouver, BC, Canada
[4]Department of Electrical and Computer Engineering, University of British Columbia, Vancouver, BC, Canada
[5]Department of Urologic Sciences, University of British Columbia, Vancouver, BC, Canada

E-mail: Piotr.Kozlowski@ubc.ca

***Introduction*:** Prostate cancer remains the most common noncutaneous malignancy in North American males and second leading cause of cancer related deaths in men. Owing to the widespread use of screening tests many more prostate tumours are being detected, many of which are less advanced, localized, lower risk cancers. This prompted increased interest in focal therapy as an alternative to the traditional therapies of radical prostatectomy and radiation therapy. The ultimate success of focal therapy relies on proper patient selection and adequate characterization of the tumour's location, extend and histological grade. Our results presented here demonstrate multi-parametric MRI capability of accurate characterization of prostate tumours.

***Materials and Methods*:** Patients with a high clinical suspicion for prostate adenocarcinoma due to an elevated prostate specific antigen (PSA) and/or palpable prostatic nodule, with no prior treatment, underwent combined DTI/DCE MRI examination on a 3 T MRI scanner prior to transrectal ultrasound (TRUS)-guided biopsies. MRI parameters (ADC, FA, K^{trans}, v_e, v_p) were correlated with the biopsy and prostatectomy results. logistic regression (LR) and support vector machines (SVM) analyses were used to estimate the diagnostic accuracy of the combined MRI techniques and to predict the location, extend and Gleason score of the tumours.

***Results and Discussion*:** Both LR and SVM analyses showed that the combination of DTI and DCE MRI has significantly better accuracy in prostate cancer diagnosis than either technique alone, with the area under the ROC curve reaching 0.96 for the combined MRI parameters. The Spearman Rank Correlation Coefficient test showed statistically significant correlation between the Gleason score and the ADC (rho = -0.661, $p = 0.0005$), and FA (rho = -0.551, $p = 0.0036$), with the LR analysis showing statistically significant dependence between the Gleason score and the MRI parameters ($p < 0.0001$ for the model).

SVM analysis generated cancer probability maps that accurately predicted the location of a dominant lesion, as verified by histology sections. The cancer probability also correlated with the Gleason score. The accuracy of predicting tumour volume by the cancer probability increased with the Gleason score of the tumour.

Our results strongly suggest that multi-parametric MRI is capable of accurately characterizing prostate cancer and indicate the potential of this technology in outlining the dominant tumour for patient selection and subsequent monitoring of focal treatment.

Key words: Prostate cancer; Multi-parametric MRI; Gleason score; Focal therapy.

A Study of the Combined Effects of Radiation Therapy and High-Intensity Focused Ultrasound Mediated Microbubble Exposure in a Tumour Mouse Model

Priscilla Lai[3,4], Justin Lee[1,2,3,4], Gregory J. Czarnota[1,2,3,4]

[1]Radiation Oncology, Sunnybrook Health Sciences Centre, 2075 Bayview Avenue, Toronto, Ontario, Canada M4N 3M5

[2]Department of Radiation Oncology, University of Toronto, 2075 Bayview Avenue, Toronto, Ontario, Canada M4N 3M5

[3]Imaging Research, Sunnybrook Health Sciences Centre, 2075 Bayview Avenue, Toronto, Ontario, Canada M4N 3M5

[4]Department of Medical Biophysics, University of Toronto, 2075 Bayview Avenue, Toronto, Ontario, Canada M4N 3M5

E-mail: Priscilla.lai@sunnybrook.ca

***Introduction*:** Recent studies have demonstrated that ultrasound-activated microbubbles (MBs) may cause biological alterations in the vascular system. Many of the changes observed included vascular lesions, endothelial cell damage or death, vascular permeability and integrity, and hemorrhaging. The results of these studies suggest that MBs have therapeutic applications that extend beyond the diagnostic purposes for which they were originally designed. However, few studies have investigated the effectiveness of MBs in combined therapies, particularly the use of MBs as a vascular radiosensitizer. The objective of this study was to address the efficacy of high-intensity focused ultrasound (HIFU) mediated MBs as a form of vascular targeted treatment when coupled with radiation, leading to secondary cell death in a pre-clinical tumour mouse model. The overall tumour response and occurrence of apoptosis from microbubble induced mechanical stress combined with radiation therapy was of interest.

***Materials and Methods*:** A human adenocarcinoma breast cell line (MDA-MB-231) from the American Type Culture Collections (ATCC, MD, USA) was used. Female immunodeficient Swiss Nude mice (Charles River Laboratory International Inc. Canada) were injected subcutaneously into the right hind leg. The ultrasound contrast agent used for these experiments was Definity® (Lantheus Medical Imaging, Inc., North Billerica, MA, USA). In this time dependent study, mice were selected at random for each treatment group. Four MB concentrations, nil (0%), low (0.5%), medium (1%) and high (3%), and three radiation doses, 0 Gy, 2 Gy and 8 Gy, were investigated and compared to the control group. The animals were divided into short term cohorts (3 hr, 12 hr, and 24 hr) and long term cohorts (<30 days). Colony forming assays were conducted on the 3 hr cohort to investigate the cancer cell viability of different treatment groups. A tumour growth delay study was conducted on the long term cohort to determine differences in rate of change in tumour volume post treatment. Tumour specimens were stained using terminal deoxynucleotidyl transferase (TdT) mediated dUTP nick end labelling (TUNEL), hematoxylin and eosin (H&E), and cluster of differentiation 31 (CD31), and the cell death subsequently quantified.

***Results and Discussion*: Histological Quantification of Cell Death.** 2 Gy radiation exposure results in a greater extent of damage in comparison to 8 Gy when coupled with MBs and ultrasound therapy. This finding was consistent across low and high MBs concentrations suggesting that lower doses of radiation therapy are equally effective in combined treatments. The coupling of MBs with radiation led to a 2(±1) times increase in cell killing for low concentrations of MBs, and 5(±2) times increase for high concentrations of MBs. **Clonogenic Survival.** Two groups, 2 Gy/high MBs and 0 Gy/high MBs, yielded survival fractions above 100% indicating that MBs, when coupled with low doses of radiation, increase the viability of cells within the tumour and stimulates growth. The remainder of the treatment groups' survival fractions (SFs) was below 40%, demonstrating that these treatment combinations were successful in reducing the self-renewal capabilities of the cancer cells. **Tumour Growth Delay.** Tumours receiving 8 Gy/high MBs and 2 Gy/high MBs exhibited a decrease in volume in addition to a delay in growth compared to the control. These tumours returned to their original volume (at day 0) after 7-10 days post treatment.

Key words: Microbubbles; High intensity focused ultrasound (HIFU); Radiotherapy; Vasculature; Tumour.

Using Cell Penetrating Peptides to Increase Cellular Uptake of Gold Nanoparticles to Enhance Radiosensitivity

Caitlin Latimer[3], Jean-Philippe Pignol[2,3], Jean Gariépy[1,3]

[1]Imaging Research, Sunnybrook Health Sciences Centre, Toronto, ON, Canada, M4N 3M5

[2]Radiation Oncology, Sunnybrook Health Sciences Centre, Toronto, ON, Canada, M4N 3M5

[3]Departments of Medical Biophysics, University of Toronto, Toronto, ON, Canada, M4N 3M5

E-mail: Caitlin.latimer@utoronto.ca

***Introduction*:** Cationic CPPs (cell penetrating peptides) are a class of peptides which are positively charged molecules (rich in lysines and arginines). These short peptide sequences have been shown to translocate across plasma membranes, and have been proven to have the ability to carry a cargo across them. This feature will be exploited for the delivery of gold nanoparticles. Gold is a biocompatible, highly electronegative, high atomic number metal. Gold nanoparticles can be used to create an increase in radiosensitivity when irradiated as they release Auger electrons. The irradiative potential of Auger electrons are distance limited to a cell diameter. CPPs will increase the quantity of gold nanoparticles within a tumour site, as compared to passive uptake of an unlabelled gold, thus producing a robust increase in cell killing.

***Materials and Methods*:** A conjugate composed of an eight arginine CPP, a polyethylene glycol (PEG) spacer and a 30 nm gold nanoparticle were assembled for the purpose of testing our hypothesis. These molecules will be tested for their ability to enter cells and cause cell death. Once cellular uptake and cytotoxicity are optimized, these molecules will be applied to cells, along with required control and comparison treatments. The cells will be irradiated at 300 kVp, at a range of doses (0-8 Gy). The cell survival will be determined by performing clonogenic assays.

***Results and Discussion*:** The desired outcome of this work is an increase in the radiosensitivity of cells treated with the CPP labeled gold nanoparticles, as compared to cells which have been treated with an unlabeled gold, a CPP alone, or irradiation alone.

Key words: Cell penetrating peptides; Gold nanoparticles; Radiosensitivity.

Defining the Optimal Use of Gold Nanoparticles for Radiosensitization: A Monte Carlo Study

Eli Lechtman[1], Shahram Mashouf[1], Jean-Philippe Pignol[1,2]

[1]Department of Medical Biophysics, University of Toronto, Toronto, ON, Canada, M4N 3M5

[2]Sunnybrook Health Sciences Centre, Department of Radiation Oncology, Toronto, ON, Canada, M4N 3M5

E-mail: eli.lechtman@sunnybrook.ca

***Introduction*:** Gold nanoparticles (AuNPs) are currently being investigated as novel high-Z radiosensitizing agents. Experimental studies of AuNP radiosensitization reveal the radiobiological effect to be highly sensitive to a number of physics and pharmacological parameters including irradiation energy and AuNP size, concentration, and intracellular localization. In this Monte Carlo simulation study we explored the interplay of these parameters on AuNP radiosensitization in order to define the optimal use of AuNPs as part of a potential clinical strategy.

***Materials and Methods*:** Monte Carlo Simulations were performed with MCNP-5 and Penelope 2008. The metrics studied included the rate of photoelectric absorption in AuNPs of various sizes (1.9, 5, 30, and 100 nm diameter), the subsequent dose enhancement in the surrounding tissue, and the energy and range of the escaping electron cascade. Clinical photon sources were studied including permanent brachytherapy seeds ^{103}Pd, ^{125}I; high dose rate brachytherapy sources ^{169}Yb, ^{192}Ir; and external beam sources 300 kVp, and 6 MV.

***Results and Discussion*:** We observed an increase of three orders of magnitude in the rate of photoelectric absorption in AuNPs using a ^{125}I brachytherapy source compared to a 6 MV source. Results indicated that to double the prescribed dose to a tumour using a ^{125}I source, concentrations of 5.33-6.26 mg g^{-1} of Au or 7.10×10^4 30 nm AuNPs per tumor cell would be required. For a 6 MV source, concentrations of 1560-1760 mg g^{-1} or 2.17×10^7 30 nm AuNPs per cell would be needed. Electrons escaping AuNPs using the lower energy sources were observed to travel distances on the order of microns, while electrons escaping AuNPs using higher energy sources traveled hundreds of microns.

From these results we have outlined two potential clinical strategies. The first strategy for AuNP radiosensitization in conjunction with photon energies below the k-edge would aim to take advantage of the extremely localized low energy

Auger cascades and would involved AuNPs of 5 nm or less conjugated to tumour target moieties and nuclear localising sequences. The second clinical strategy in conjunction with photon energies above the k-edge would require a higher concentration of gold in the tumor. In this approach, AuNP size and localization are less relevant, and energy from longer ranged photoelectrons would be the main contribution to radiosensitization.

Key words: Radiation therapy; Gold nanoparticles; Radiosensitization; Monte carlo simulation.

Microbubble and Ultrasound Enhancement of Radiation-Induced Tumour Cell Death *In Vivo*

Czarnota G. J.[1,2], Lee J.[2], Karshafian R.[3], Giles A.[1], Iradji S.[1], Wong E.[1], Al Mahrouki A.[1]

[1]Imaging Research and Radiation Oncology, Sunnybrook Health Sciences Centre, Toronto, ON, Canada, M4N 3M5

[2]Departments of Radiation Oncology and Medical Biophysics, University of Toronto, Toronto, ON, Canada, M4N 3M5

[3]Ryerson University, Department of Physics, Toronto, Ontario, Canada, M5B 2K3

E-mail: justin.lee@sunnybrook.ca

***Introduction*:** It is now appreciated that radiation not only damages the DNA inside tumour cells *in vivo* but may act by damaging the endothelial cells of the vasculature. In this study we tested the hypothesis that microbubble agents *in vivo* may be used *a priori* to cause endothelial cell perturbations thus causing "radiosensitization" of tumours.

***Materials and Methods*:** Human prostate cancer xenograft-bearing mice (260 animals) were exposed to combinations of ultrasound, activated-microbubbles, and radiation (8 animals per group). For ultrasound treatments, animals were exposed to 16 cycles tone burst at 500 kHz center frequency 570 kPa peak negative pressure with a 3 kHz pulse repetition frequency for 5 minutes. For treatments involving bubbles, Definity bubbles (Bristol Myers-Squibb) were first administered and for radiation treatments 160 kVp X-rays were used at doses of 2 and 8 Gy and with multiple treatments over 3-4 weeks (60 animals). Representative tumour sections were examined using immunohistochemistry. Clonogenic assays and growth delay studies were also carried out.

***Results and Discussion*:** Analyses indicated a synergistic increase in tumour cell kill due to vascular disruption caused by the combined therapies that increased when microbubbles were used in conjunction with radiation with increases of cell kill from 5% to over 50% with combined single treatments. Immunohistochemistry indicated endothelial cell apoptosis and activation of the ceramide cell-death pathway to be caused by microbubbles. Multiple treatments indicated better therapeutic outcome with multiple treatments combining both modalities compared to single modality treatments.

***Conclusions*:** Radiation effects were synergistically enhanced by using microbubbles to perturb tumour vasculature prior to the administration of radiotherapy. Analyses indicated activation of ceramide-mediated apoptotic cell death in endothelial cells leading to vascular disruption in tumours. This lead to profoundly enhanced tumour cell death even after one combined treatment using a 2 Gy radiation dose. This work forms the basis for ultrasound-induced spatial targeting of radiotherapy enhancement.

Key words: Apoptosis; Ceramide; Ultrasound.

Microbubble Contrast Ultrasound to Monitor *In Vivo* Tumor Perfusion in Response to Notch Pathway Inhibitors

Stanley K. Liu[1], Emmanouil Fokas[2], Saif A. Bham[2,3], Adrian L. Harris[2,3,4], Ruth J. Muschel[2,4]

[1]Sunnybrook Research Institute, Sunnybrook Health Sciences Centre, and Departments of Radiation Oncology and Medical Biophysics, University of Toronto, Toronto, ON, Canada

[2]Gray Institute for Radiation Oncology & Biology, Radiobiology Research Institute, Oxford, UK and University of Oxford, Oxford, UK

[3]Weatherall Institute of Molecular Medicine, Molecular Oncology Unit, University of Oxford, Oxford, UK

[4]Denotes Equally Shared Senior Authorship

E-mail: stanley.liu@sunnybrook.ca

***Introduction*:** The microenvironment plays an important role in regulating tumor response to radiotherapy. There is great interest in the use of novel agents that modify the tumor microenvironment in combination with ionizing radiation (IR), to improve tumor control. IR can disrupt tumor

vasculature, and given that Notch pathway inhibition can interfere with functional angiogenesis, there is a strong rationale to explore its potential cooperativity with IR in delaying tumor growth.

***Materials and Methods*:** Human colorectal carcinoma cells (LS174T) expressing a Notch luciferase reporter were grown as subcutaneous xenografts in nude mice and treated with a specific anti-DLL4 blocking antibody (DLL4 mAb), solely or in combination with IR, and tumor growth delay determined. Correlative studies included microbubble contrast Doppler ultrasound to measure tumor perfusion, *in vivo* bioluminescence to monitor tumor Notch activity, confocal imaging of tumor vasculature and immunohistochemistry.

***Results*:** DLL4 mAb given solely or in combination with IR resulted in decreased tumor perfusion and increased tumor vessel density but paradoxically reduced tumor perfusion, consistent with non-functional angiogenesis. This resulted in significant tumor necrosis and supra-additive tumor growth delay, which was well-tolerated.

***Conclusions/Future Plans*:** This novel approach of combining specific DLL4-Notch blockade with IR for impairing tumor growth by promoting non-functional tumor angiogenesis and extensive tumor necrosis is expected to be broadly applicable to solid tumors, and provides support for testing this within the context of an early phase clinical trial. Additionally, tumor perfusion inhibition as assayed by contrast ultrasound may serve as a useful biomarker for monitoring cancer patients undergoing Notch inhibitor therapy.

Key words: DLL4; Notch pathway; Angiogenesis; Ionizing radiation; Doppler ultrasound.

Real-Time and Non-Invasive Optical Imaging of Tumor and Vascular Response to Ionizing Radiation *In Vivo*

Azusa Maeda[1], Leigh Conroy[1], Michael K. K. Leung[1], Emily Chen[2], Patricia Lindsay[2,3], David A. Jaffray[1,2,3], Richard P. Hill[1,2,3], I. Alex Vitkin[1,2,3], Ralph S. DaCosta[1,2,3]

[1]Department of Medical Biophysics, University of Toronto (UofT), Toronto, Canada

[2]Ontario Cancer Institute, University Health Network

[3]Radiation Medicine Program, UofT, Toronto, Canada

E-mail: rdacosta@uhnreserach.ca

***Introduction*:** Radiation therapy (RT) plays a central role in cancer treatment. However, experimental studies aimed to understand interdependent radiobiological response of tumor cells and their vascular networks have been impeded by a lack of imaging techniques capable of visualizing changes microscopically in real-time, non-invasively and longitudinally within solid tumors *in vivo*. To address this need, we have developed an integrated system to monitor radiobiological response of multiple biological components *in vivo*.

***Materials and Methods*:** We have combined a small animal x-ray micro-irradiator and an intravital multimodal optical imaging platform (fluorescence confocal microscopy, speckle-variance optical coherence tomography (svOCT)) to directly and simultaneously visualize individual tumor components responding to RT over time. To demonstrate the robustness and capability of our new experimental platform, we investigated the serial use and *in vivo* tolerability of multiple molecularly-targeted fluorescent agents to study specific radiobiological events in tumors, vasculature and surrounding tissues following single fraction RT (Figure 1A and 1B).

***Results and Discussion*:** Preliminary experimental validation of the platform revealed spatio-temporal events at multiple levels (cellular, structural, functional) in response to RT. Specifically, we observed and quantified changes in the relative amount of perfused blood vessels following a focal single fraction RT dose of 30 Gy. These vascular changes preceded any apparent tumor cell response. Furthermore, intratumoral vascular density increased significantly 14-18 days following RT, signifying classical RT-induced angiogenesis (Figure 1C). Our platform also allowed visualization of cellular events, such as endothelial cell death and thrombus formation following RT at capillary levels. Together, this toolset provides a new way of monitoring multiple quantitative tumor and vascular metrics (morphological, architectural, functional, and cellular) non-invasively and dynamically for preclinical radiobiological studies.

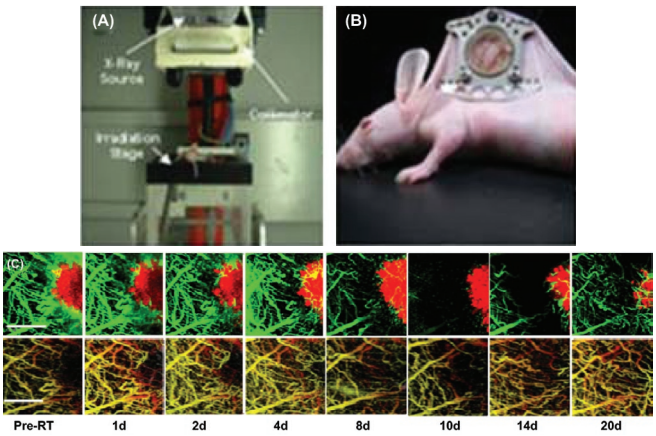

Figure 1: (**A**) The x-ray micro-irradiator system (**B**) Mouse bearing dorsal skinfold window chamber for intravital imaging (**C**) longitudinal optical imaging of irradiated tumor using fluorescence confocal microscopy (top) and svOCT (bottom), demonstrating functional and structural changes of tumor vasculature following 30 Gy RT.

Key words: Radiation therapy; Optical imaging; Tumor response; Intravital imaging; Small animal x-ray microirradiator; Tumor vasculature.

High-Frequency Quantitative Ultrasound for Detecting Lymph-Node Metastases

Jonathan Mamou[1], Ernest J. Feleppa[1], Emi Saegusa-Beecroft[2], Alain Coron[3], Michael Oelze[4], Tadashi Yamaguchi[5], Junji Machi[2], Masaki Hata[2], Eugene Yanagihara[2], Pascal Laugier[3]

[1]F. L. Lizzi Center for Biomedical Engineering, Riverside Research Institute, New York, NY

[2]Department of Surgery, University of Hawaii and Kuakini Medical Center, Honolulu, HI

[3]Laboratoire d'Imagerie Paramétrique UMR7623, CNRS - Université Pierre et Marie Curie - Paris, France

[4]Bioacoustics Research Laboratory, Department of Electrical and Computer Engineering, University of Illinois, Urbana, IL

[5]Research Center for Frontier Medical Engineering, Chiba University, Chiba, Japan

E-mail: jmamou@riversideresearch.org

***Introduction*:** A reliable means of detecting metastases in regional lymph nodes is essential for accurate staging of cancer and effective planning of therapy. Standard, current, time-consuming histopathology methods appear to have high false-negative rates for metastases that are 2 mm or smaller. We are investigating high-frequency (HF) quantitative ultrasound (QUS) methods to provide a rapid and reliable means of detecting metastases in dissected nodes based on their ultrasound-scattering properties.

***Materials and Methods*:** We acquired HF ultrasound and histological data from lymph nodes dissected from patients with colorectal, breast, gastric, and other cancers. Freshly dissected nodes were scanned in a saline water bath using a raster pattern to acquire 3-D RF echo-signal data. Scans utilized a broadband, F-2, 25.6-MHz, single-element transducer with scan vectors separated by 25 µm in X and Y directions. Scanned nodes were color inked to provide references for subsequent orientation, then fixed and serially-sectioned in their entire volume at 50-µm intervals. The presence of metastatic foci was determined histologically in every section, including the center section for comparison with conventional methods.

To date, we have analyzed the echo signals of more than 240 nodes including abdominal nodes of colorectal and gastric cancer patients and axillary nodes of breast-cancer patients. 3-D images generated from RF data were segmented semi-automatically to select nodal tissue for analysis. Echo signals from nodal tissue were processed to yield QUS estimates, which included B-mode envelope-signal statistical features.

***Results and Discussion*:** Different histological node architectures were observed and different QUS results were obtained for abdominal compared to axillary nodes. Linear discriminant analysis and ROC-curve methods were applied to assess the ability of spectral parameters, scatterer-property estimates, and statistical features to distinguish cancerous from non-cancerous nodes. Classification performance was assessed for individual estimates and various linear combinations of estimates. ROC results for axillary as well as abdominal nodes showed excellent classification. For abdominal nodes, the areas under the ROC curves approached 1.0 for a combination of all QUS estimates. Slightly poorer results were obtained for morphologically more-complex axillary nodes. Images based on QUS parameters showed an excellent ability to depict metastatic foci. These encouraging initial results suggest that HF QUS methods can provide a clinically valuable means of detecting small metastatic cancers in dissected lymph nodes that might not be detected using standard pathology procedures. The ability of HF QUS to reveal otherwise missed metastases will enable pathologists to more-efficiently focus histological effort on cancer-containing regions of nodes and therefore will improve the staging of cancer and the planning of cancer treatment. Future studies will investigate the applicability of these methods for detecting nodal metastases *in situ*. *In situ* application of these methods would provide a means of targeting metastatic nodes for dissection and monitoring node status during chemotherapy or active surveillance.

Key words: Lymph nodes; Sentinel nodes; Metastases; Micrometastases; Cancer detection; Cancer staging; Cancer monitoring.

Optimization of Breast Permanent Seed Implant Dosimetry Incorporating Tissue Heterogeneity

Shahram Mashouf[1], Eli Lechtman[1], Jean-Philippe Pignol[1,2]

[1]Department of Medical Biophysics, University of Toronto, Toronto, ON, Canada, M4N 3M5

[2]Sunnybrook Health Sciences Centre, Department of Radiation Oncology, Toronto, ON, Canada, M4N 3M5

E-mail: s.mashouf@utoronto.ca

***Introduction*:** Permanent breast seed implant (PBSI) is a new technique for adjuvant radiotherapy of early stage cancer patients. In PBSI low dose rate (LDR) ^{103}Pd radioactive seeds are implanted around the surgical cavity under light sedation using ultrasound image guidance to deliver a dose of 90 Gy. While image guidance enables a high degree of dose distribution conformity, currently the dose is calculated as if the breast medium was water (AAPM TG43). This can lead to systematic dose calculation errors up to 40%. Our work focuses on the development of more accurate dose calculation algorithms accounting for individual breast tissue composition.

***Materials and Methods*:** We used Monte Carlo simulation to evaluate the dose distribution in realistic breast tissues. Breast is composed of glandular and adipose tissues and is surrounded by air, ribs and lung, with different physical properties than water. We compared the realistic radial dose distribution away from a single ^{103}Pd seed in heterogeneous media using either the TG43 formalism, a simple density correction and a novel analytical method accounting for the mass attenuation coefficient (μ/ρ) of the media. The dose delivered to organs at risk of complication for PBSI, such as skin and lung, were compared.

***Results and Discussion*:** There are large dose variations due to the heterogeneities of breast tissue when comparing dose in water (TG43) to realistic dose distributions. The novel analytical method accounts for the variation in density and the physics of interaction of radiation with matter. By introducing necessary corrections, dose to skin and other critical organs are estimated more accurately, which enables a more personalized dose distribution and treatment. It is hypothesized that a more accurate dose calculation could result in a lower rate of treatment complication, including acute moist desquamation, permanent skin telangiectasia and painful induration.

Key words: Personalized breast radiotherapy; Accelerated partial radiation; Brachytherapy.

Dynamic Contrast Enhanced (DCE)-CT and -MR Imaging in Cervical Cancer

Michael Milosevic

University of Toronto Department of Radiation Oncology, and Radiation Medicine Program, Princess Margaret Hospital – University Health Network, Toronto, Ontario, Canada

E-mail: mike.milosevic@rmp.uhn.on.ca

Angiogenesis is a prominent feature of invasive cervical cancer, as evidenced from histopathologic and functional studies. High expression of hypoxia inducible factor (HIF), carbonic anhydrase IX (CAIX) and other tissue-based biomarkers of angiogenesis have been associated with poor clinical outcome after treatment with radiotherapy (RT). High interstitial fluid pressure (IFP), an integrated measure of vascular and lymphatic dysfunction in tumors, has been linked to disease recurrence both in the pelvis and at metastatic sites. DCE-MR and -CT offer the potential to interrogate vascular characteristics in patients with cervical cancer in a minimally invasive and repeatable manner. Studies in cervical cancer have shown substantial differences in DCE-CT and -MR parameters between tumor and normal muscle in keeping with higher blood flow and vascular permeability, and substantial variation in these parameters from one tumor to the next and within individual tumors. Despite the potential to indentify cervical cancers with different vascular characteristics, the results of studies evaluating the relationship between DCE imaging prior to RT and clinical outcome have been inconsistent. This in part reflects a lack of consensus on the optimal imaging technique, analysis method and reporting metric with greatest biologic relevance and clinical utility. Treatment-related changes in DCE imaging parameters may provide more relevant information, especially in an era where RT is increasingly being combined with drugs that target the tumor vasculature or other biologic pathways, to enhance treatment response. For example, the addition of the anti-angiogenic drug sorafenib to standard RT for patients with cervical cancer at Princess Margaret Hospital yielded DCE-MR changes consistent with reduced perfusion and/or vascular permeability and an increase in tumor hypoxia, suggesting that sorafenib is unlikely to improve clinical outcome in these patients. Further refinement and standardization of DCE imaging could in the future support adaptive treatment strategies where RT either alone or in combination with biologic targeting is continuously optimized over a course of treatment to maximize patient benefit.

Key words: Cervical cancer; Radiotherapy; DCE-CT; DCE-MR.

Physical Co-Registration of DCE-MRI and DCE-US Data in a Murine Tumour Model

Firas Moosvi[1,2], Melissa Yin[1], Greg Stanisz[1,2]

[1]Imaging Physics, Sunnybrook Health Sciences Centre, Toronto, ON, Canada, M4N 3M5

[2]Department of Medical Biophysics, University of Toronto, Toronto, ON, Canada, M5A 2N4

E-mail: firas@moosvi.com

***Introduction*:** The use of complementary non-invasive imaging modalities has been proposed to track disease progression, while simultaneously evaluating therapeutic efficacy. However, a major obstacle is a limited ability to compare parameters obtained from different modalities, especially those from exogenous contrast agents or tracers. We propose to bypass a number of challenges associated with multi-modality imaging with an *a priori* image co-registration technique between MR and US data accurate to within 0.25 mm in-plane and 0.5 mm through-plane. We hypothesize that by using this technique, using DCE-MRI in combination with DCE-US will extend non-invasive characterization of tumours and facilitate a more complete analysis of the tumour microenvironment during treatment.

***Materials and Methods*: Mice.** Twelve (12) nude SCID mice from Charles River were injected with Lewis Lung Carcinoma cells subcutaneously and allowed to grow to a diameter of 1 cm, anesthetized using a ketamine/xylazine cocktail and imaged sequentially. **Apparatus.** A physical co-registration apparatus was designed to enable co-planar MR and US imaging. Acoustic waves transmitted from a transducer located above the apparatus are coupled to a water tank placed between the mouse and the transducer. A 1-mm thin staircase-shaped insert fixed in the water tank provided a reference plane for *a priori* image co-registration (Figure 1). **MRI.** Imaging was performed using a 7T Bruker system with a volume coil. Two sequences (2D FSE and 3D FSPGR) were used to acquire data. Temporal resolution of DCE-MRI was 11 s with full tumour coverage. **Ultrasound.** US imaging was performed using the Vevo 2100 scanner (VisualSonics) operating at a centre frequency of 21 MHz. The staircase insert was used to align the US transducer at the same reference plane as MRI, and slices were acquired in a sagittal orientation, 1 mm apart. The mice were continuously infused with microbubbles (MicroMarker; VisualSonics, Toronto, ON) and DCE-US data was acquired at a temporal resolution of 0.2 s. **Enhancement Maps.** A pixel-by-pixel map of signal enhancement was calculated by taking the ratio of the signal intensity after contrast injection (MRI) or infusion (US) and the baseline signal intensity. The numbers in the colour maps in Figure 2 correspond to how many times a pixel enhanced relative to the baseline intensity at that pixel.

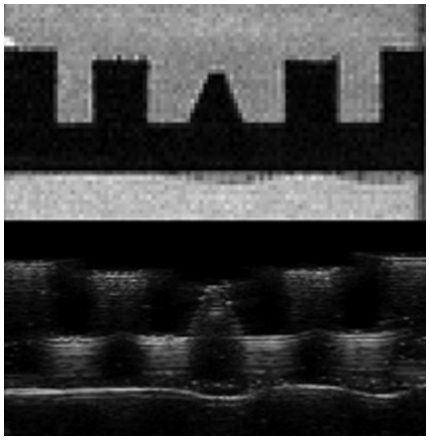

Figure 1: Fixed fiducial marker visible in both MR (top) and US (bottom).

***Results and Discussion*:** This protocol facilitates dynamic contrast enhanced co-planar multi-modality imaging in mouse tumours. The use of both intravascular (US microbubbles) and extravascular (MRI tracers) contrast agents used together presents a unique opportunity to study the tumour miroenvironment more thoroughly. From the sample case shown in Figure 2, we note that enhancement in this particular tumour is fairly homogenous suggesting that the tumour is likely well-vascularized. The next step in this project is to introduce a treatment and quantitatively assess changes in enhancement due to treatments.

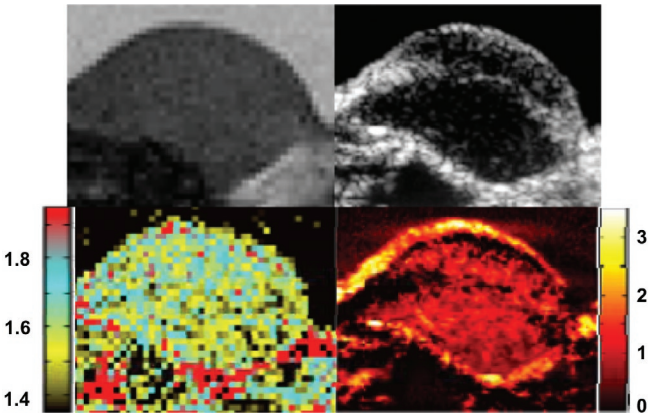

Figure 2: High resolution anatomical images acquired with MRI (top left) and ultrasound (top right). The DCE-MRI enhancement map (bottom left) shows near homogenous enhancement in the tumour, with some regions of hyper intensity, possibly due to the presence of larger vessels. The DCE-US enhancement map (bottom right) shows a similar trend with most of the tumour enhancing (red) and since the contrast agent is intravascular, avascular regions appear black.

Key words: DCE-MRI; DCE-US; Microbubbles; Tumour; Registration.

Acoustic Radiation Force Based Imaging of Cancer

Kathryn Nightingale, Veronica Rotemberg, Taylor Jordan, Xuan Cao, Ned Rouze, Christina Hsu, Mark Palmeri, Liang Zhai, Fan Yuan

Department of Biomedical Engineering, Duke University, 27708-0281, Durham, NC, USA

E-mail: kathy.nightingale@duke.edu

***Introduction*:** Acoustic radiation force based elasticity imaging methods are under development for the purpose of detecting, characterizing, and longitudinally monitoring the stiffness of malignant tumors. In this approach, temporally impulsive (*i.e.* <1 msec) focused acoustic radiation force is used to mechanically excite tissue, and the dynamic displacement response is monitored using the same transducer and ultrasonic correlation based techniques. High resolution qualitative images can be generated that portray relative differences in tissue stiffness, maintaining structural integrity in heterogeneous media. These images are generated by monitoring the tissue response along the central axis of the excitation, and sequentially interrogating a 2D (or 3D) field of view (*i.e.* on-axis, or ARFI imaging). Shear wave imaging methods have also been employed to quantify the shear wave speed (SWS) of the shear waves generated by the impulsive excitation. While this approach provides quantitative stiffness information, it suffers from inherently lower resolution than the on-axis method, and, it is also subject to a class of artifacts arising from shear wave reflections in heterogeneous media. We have developed a combined approach that achieves the structural integrity and high resolution of the on-axis method while also providing quantitative information. We will present data from two ongoing studies: 1) a pilot study in patients who are known to have prostate cancer and have elected to have radical prostatectomy, in which correlation between pre-surgical ARFI elasticity images and the corresponding *ex vivo* whole mount histology is performed in order to determine what is visible in ARFI prostate images and 2) a small animal study in which we are applying the combined method to determine the potential for longitudinal monitoring of changes in stiffness with tumor growth in both a melanoma and a breast cancer model.

***Materials and Methods*:** For the prostate cancer study, we utilize a modified, research dedicated Siemens Antares scanner and an EV9F4 transducer (end-fire, curvilinear, mechanical wobbler) to obtain 3D ARFI data from the entire prostate volume immediately prior to radical prostatectomy surgery. We then perform whole-mount histological sectioning of the prostate post-excision. The histology images are read by a pathologist blinded to the ARFI findings, and the ARFI images are correlated with the histological results. For the small animal tumor study, tumor cells are implanted in the mouse hind limb, and imaging is performed at multiple time-points as the tumors grow, typically separated by 48 hours, starting when the tumors are 5 mm in diameter. This study is performed with a 14L5 transducer and a modified, research dedicated Siemens S2000 imaging platform.

***Results and Discussion*:** ARFI images of the prostate portray zonal anatomy (peripheral zone, central gland, urethra, ejaculatory ducts) with high contrast. Prostate cancer, when visible, appears as stiff, asymmetric regions in coronal ARFI images. BPH, which develops in the transition zone (or central gland) has a nodular appearance, with both soft and stiff nodules. The stiffer nodules can appear similar to cancerous lesions. Examples of the different pathologies will be presented. For the ongoing mouse tumor study, results comparing the combined high resolution quantitative imaging approach in the two tumor types at multiple time points during tumor growth will be presented. These data suggest promise for ARFI imaging in the context of targeting prostate biopsy and focal therapy procedures, and for quantifying changes in tumor stiffness with disease progression.

Key words: Acoustic radiation force; Elasticity imaging; Shear modulus; Cancer imaging.

Quantitative Ultrasound

William D. O'Brien, Jr.

Bioacoustics Research Laboratory, Department of Electrical and Computer Engineering, University of Illinois, 405 N. Mathews, Urbana, IL 61801, USA

E-mail: wdo@uiuc.edu

***Introduction*:** Our early work to develop a basis for quantitative ultrasound (QUS) imaging started with live animal studies wherein the ultrasonic backscattered coefficient (BSC) was estimated and from the BSC estimate, QUS parameters were estimated. Even earlier (some 5 decades earlier), significant through-transmission quantitative studies of ultrasonic tissue properties were undertaken (absorption and speed). It was our view, based on the significant early echo-based work by Lizzi *et al.*, Zagzebski *et al.*, Insana *et al.*, and Hall *et al.*, that QUS imaging technology had the potential to be a new imaging capability that could be used to augment standard B-mode imaging.

***Materials and Methods*:** QUS imaging utilizes the frequency-dependent information, and thus the backscattered signals are dependent on the tissue properties (size, shape, number, compressibility, density). Estimating QUS parameters requires a model that incorporates a form factor (FF), that is, a mathematical description/model of the backscattered signal of a single scattering structure as a function of frequency; the better the FF describes anatomical scatterers, the more realistic will be the estimates.

***Results and Discussion*:** We initiated our studies by examining *in vivo* three solid tumor types (fibroadenoma, mammary carcinoma, soft-tissue sarcoma). Initially the Gaussian FF was used. Good agreement between processed ultrasound data and pathologic assessments were obtained, but also, important questions were being raised. The questions lead to new approaches to identify more accurate FFs, as well as new strategies to extract quantitative parameters from the envelop-detected echo data. The presentation will provide the basis for QUS based on our early work as well as our on-going work that includes various cell pellet preparations (biophantoms) and *in vivo* tumors using data acquired from array-based imaging systems. [Supported by NIH CA111289]

Key words: Quantitative ultrasound; Ultrasonic backscattered coefficient; Form factor; Biophantoms; *In vivo* tumors.

Use of Ultrasound to Enhance Therapy and Detect Therapeutic Response

Stanley Swat[1], Jeremy Kemmerer[2], Goutam Ghoshal[2], Michael L. Oelze[2]

[1]University of Illinois at Urbana-Champaign, Department of Molecular and Cellular Biology, Urbana, Illinois, USA, 61801

[2]University of Illinois at Urbana-Champaign, Department of Electrical and Computer Engineering, Urbana, Illinois, USA, 61801

E-mail: oelze@illinois.edu

***Introduction*:** Ultrasound is a unique form of radiation in that it can be used for imaging and therapy, often with the same device. In this talk, an ultrasound-enhanced therapy technique will be discussed along with a quantitative ultrasound (QUS) imaging technique that is capable of detecting and quantifying therapy efficacy. The hypotheses to be tested is that ultrasound can synergistically enhance cell death beyond conventional methods alone and that the effects of therapy can be detected using high frequency QUS ($>$15 MHz). The ultrasound-enhanced therapy technique includes treating cells in culture using ultrasound and ultrasound contrast agents (gas-filled microbubbles) combined with chemotherapy (a single dose of doxorubicin). Complementary to this, QUS techniques were explored for detecting changes in liver tissues treated with different thermal doses.

***Materials and Methods*:** 4T1 cancer cells were grown in cell culture flasks. Before an experiment, cells were plated in 96 well plates for exposure to ultrasound. In some plates, ultrasound contrast agents were added (Definity) before ultrasound exposure. Cells in different plates were either exposed to ultrasound, ultrasound and microbubbles, or no ultrasound. Immediately after ultrasound exposure, cells were treated with doxorubicin (5.8 μg/mL or approximately 1/3 normal dose). Cells were incubated for 24 hours and then cell viability was assessed using an MTT assay. For the QUS therapy assessment, fresh liver samples were extracted from a rat, the liver samples were cut into different lobes, and the different lobes were placed in a degassed bath of saline and heated to 37, 45, 50, 55, 60, 65, or 70°C for 10 minutes. After heating, samples were placed in a bath of saline and scanned with a 20 MHz single-element transducer. QUS analysis was conducted on the backscattered data. From the backscatter coefficient, an estimate of the effective scatterer diameter (ESD) was obtained using a spherical Gaussian model.

***Results and Discussion*:** When combining microbubbles and ultrasound exposure with doxorubicin, more than a doubling of cell death (49% cell death) was observed compared to administering only a low dose of doxorubicin (24% cell death) or ultrasound and microbubble exposure alone ($<$10% cell death). For QUS detection of therapy, the backscatter coefficient provided contrast between tissues with different thermal doses. The ESD for the larger thermal doses corresponded to diameters between 18 to 25 μm while for the lower thermal doses the ESD ranged between 12 and 16 μm. From histology images, liver cell sizes for the higher thermal doses were in the range of 20-25 μm while the cell nuclei were approximately 10 μm. Ultrasound has the potential to radically alter cancer therapy by providing targeted therapies and requiring lower doses of potentially toxic therapy and QUS techniques are poised to detect and quantify the efficacy of cancer treatment noninvasively.

Key words: Quantitative ultrasound; Hyperthermia; HIFU; Chemotherapy; Ultrasound contrast agents.

Material Property of Soft Tissue Measurement Using Ultrasound Excitation and Optical Coherence Elastography

Marjan Razani[1], Cuiru Sun[2], Adrian Mariampillai[2], Victor X. D. Yang[2], Michael C. Kolios[1]

[1]Department of Biophysics, Ryerson University, Toronto, Canada

[2]Department of Electrical and Computer Engineering, Ryerson University, Toronto, Canada

E-mail: mrazani@ryerson.ca

***Introduction*:** Elastography is a method in which stiffness or strain images of soft tissue, called elastograms, are generated for diagnostic purposes. Elastograms contain information about local variations of the stiffness inside a region of interest and may provide additional clinical information to aid identification of suspicious lesions, the diagnosis of various disease states or for treatment monitoring. Different imaging modalities can be used to image tissue displacement and generate elastorgrams such as ultrasound or magnetic resonance imaging (MRI). However both MRI and ultrasound do not have sufficient resolution to detect small and subtle elastic variations in tissue such as in small tumors and atherosclerotic plaques. Optical Coherence Tomography (OCT) provides imaging in histological resolution, which allows for the identification of micron sized morphological tissue structures. Optical coherence elastography (OCE) measures tissue displacement using OCT and benefits from the high resolution of OCT to generate high-resolution stiffness maps. In this work, we explore the potential of measuring shear wave propagation using OCE. The specific aims of this work are to: 1) Design experimental methods to image tissue deformation induced by the acoustic radiation force produced by an ultrasound transducer using OCT; 2) Design algorithms to generate displacement or strain elastograms from the OCT data, and; 3) Characterize the propagation of the ultrasound shear waves generated by the "push" transducer using OCT.

***Materials and Methods*:** A swept-source OCT system was used in this study. The laser had a center wavelength of 1310 nm and a bandwidth of ~110 nm. The lateral resolution was approximately 13 μm in the samples. Acoustic radiation force was applied by a 20 MHz circular 8.5 mm diameter piezoelectric transducer (PZT) element transmitting sine-wave bursts of 400 μs. Gelatin-based phantoms (Type B gelatin, with 5% and 10% w/w gel concentrations) were constructed for measurement of displacement. A 355 μm glass sphere was embedded at the center of the gelatin phantom. The focus of the ultrasound beam was positioned at the location of the sphere. All OCE experiments were conducted within 1-2 days of gelatin phantom construction.

The ultrasound "push" transducer is synchronized with the OCT imaging systems so that there is only one ultrasound pulse generated during the acquisition of each image frame. Different time delays between the transducer activation and the initiation of the OCT imaging sequence are set to evaluate the imaging scheme. B-mode and M-mode OCT images are obtained when the ultrasound transducer is generating the "push" in the phantom. A phase analysis algorithm is used to analyze the images and characterize the movement of the tissue under ultrasound load. A fast Fourier transform was performed on the OCT data and phase maps of the phantom are generated, which are directly related to the acoustic radiation force induced displacement in the phantom.

***Results and Discussion*:** The ultrasound pushing beam was characterized in separate experiments, which laid the foundation for our final goal of imaging shear wave propagation in tissue and characterizing the tissue material properties using OCE. First, B-mode images of the sphere allowed localization of the sphere in the OCT image. M-mode OCT images were acquired at the location for which an OCT a-line from the image would cross the center of the sphere. The amplitude and phase of an M-mode image are used to track the sphere displacement. The phase of the M-mode OCT image is proportional to the displacement of the sphere over time, and was used for the elastography analysis. It was found that OCE can track the sphere displacement as a function of time. In subsequent experiments, OCE was able to track displacements adjacent to the transducer focus as the shear wave produced by the push beam propagated through the phantom. In summary, OCT can be used to track the tissue displacement produced by the acoustic radiation force of a focused ultrasound transducer.

Key words: Shear wave; Elastography; Optical coherence tomography; Transducer; Mechanical properties.

CT-Enhanced US Image of Lung's Tumor for Image-Guided LDR Brachytherapy

Ali Sadeghi-Naini[1,2], Rajni Patel[3,4], Abbas Samani[3,5,6]

[1]Departments of Imaging Research/Radiation Oncology, Sunnybrook Health Sciences Centre, Toronto, ON, Canada
[2]Departments of Medical Biophysics/Radiation Oncology, University of Toronto, Toronto, ON, Canada
[3]Department of Electrical & Computer Engineering, University of Western Ontario, London, ON, Canada
[4]Department of Surgery, University of Western Ontario, London, ON, Canada
[5]Department of Medical Biophysics, University of Western Ontario, London, ON, Canada
[6]Imaging Research Laboratories, Robarts Research Institute, London, ON, Canada

E-mail: Ali.Sadeghi-Naini@sunnybrook.ca

***Introduction*:** Low Dose Rate (LDR) Lung brachytherapy is a novel concept for minimally invasive tumor ablation. To adapt LDR brachytherapy for lung cancer therapy, a number of major imaging difficulties need to be overcome. All of these difficulties stem from the poor quality of intra-operative US images of deflated lung. Alternatively, pre-operative lung CT or MRI images are not effective in LDR brachytherapy as they are not consistent with the lung being totally deflated during surgery. To address the poor quality issue of deflated lung US images, it is possible to register the US images with higher quality images obtained pre-operatively, *e.g.* CT. However, the CT images need to be pre-processed to obtain CT images pertaining to the lung's deflated state.

***Materials and Methods*:** We proposed a solution for intra-operative imaging during a lung brachytherapy procedure. This involves constructing a CT image of the totally deflated lung using the lung's pre-operative images by means of a fully automatic technique. The technique consists of a deformable registration/air volume estimation/extrapolation pipeline. This is followed by a process to enhance the US images' poor quality using the constructed CT image. The US enhancement process utilizes a novel registration strategy which outputs a CT-enhanced US image of the totally deflated lung positioned and oriented accurately in its pre-operatively constructed CT counterpart. *Ex vivo* experiments were conducted on a porcine lung with a tumor phantom sutured inside. A 4D-CT respiratory sequence was acquired while the lung was being respired. The sequence was used pre-operatively to construct a CT image of the deflated lung where sub-millimeter accuracy was achieved according to the validation results (Figure 1A and 1B). A number of 2D US images were then acquired from the target tumor area of the deflated lung. The US images, along with the constructed CT image, were processed by the proposed method pipeline.

***Results and Discussion*:** The results showed significant quality improvement in semi real-time which led to achieving reliable and accurate intra-operative images of the deflated lung (Figures 1C-F). Obtaining accurate CT/US images of the deflated lung can address one of the major challenges encountered in LDR lung brachytherapy. It is also a substantial forward step for its implementation. Such images can be effectively applied for treatment planning, tumor intra-operative localization, and fusing with real-time navigation information, which are known to be paramount necessities for the LDR lung brachytherapy procedure.

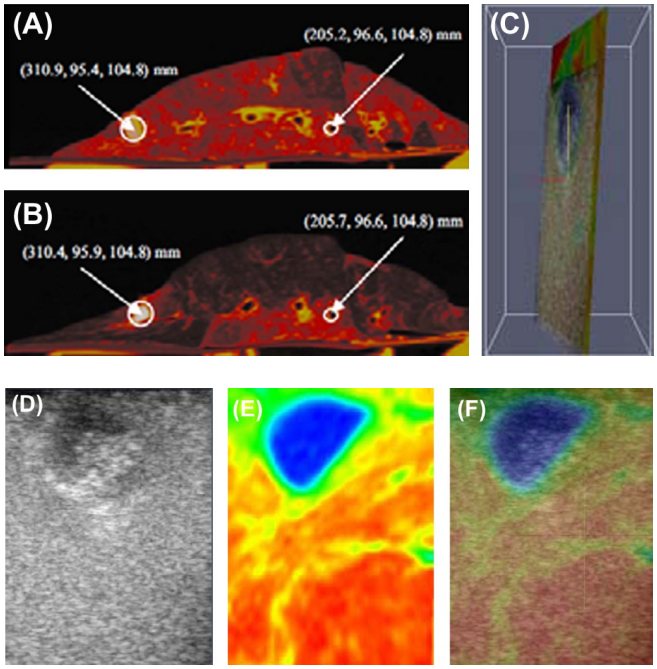

Figure 1: One tumor passing slice of the (**A**): totally deflated lung CT image (required). (**B**): constructed CT image of the deflated lung. (**C**): Optimized orientation and position of the 2D-US plane within the 3D-CT sub-volume. (**D**)-(**F**): Results of US enhancement. (**D**): intra-operative US image of the lung's tumor area. (**E**): CT enhanced version of the US image. (**F**) original US image overlaid on its CT enhanced version.

Key words: LDR; Lung brachytherapy; Deformable registration; US image enhancement; Minimally invasive procedures; Image-guided interventions.

Partial Volume Correction of Noninvasive Pet Image-Derived Simplified Kinetic Analysis for Tumor Response Assessment

Mike Sattarivand[1,2], Curtis Caldwell[1,2]

[1]Imaging Research and Radiation Oncology, Sunnybrook Health Sciences Centre, Toronto, ON, Canada, M4N 3M5

[2]Departments of Radiation Oncology and Medical Biophysics, University of Toronto, Toronto, ON, Canada, M4N 3M5

E-mail: mike.sattarivand@sunnybrook.ca

***Introduction*:** Functional imaging with positron emission tomography (PET) using fluoro-deoxy-glucose is a powerful tool in tumour response evaluation. One PET metric for tumour response assessment is the use of simplified kinetic analysis of tumour metabolism that requires a blood sample for patient's blood activity estimation. Our approach is to measure blood activity directly from the PET images without a need for the blood sample. However, due to the small size of these vessels and low resolution of PET, a partial volume correction (PVC) needs to be applied.

***Materials and Methods*:** A phantom was designed with a cylinder tank and six fillable cylinders to simulate vessels with a range of inner diameters from 4.8 to 28.6 mm. F-18 in aqueous solution was injected into the vessels and the tank with an activity concentration ratio of 1.5 to 1. The PET FOV was 576 mm and voxel size $4 \times 4 \times 4$ mm. CT images of this phantom were used to create a digital 3D PET phantom model. The inner and outer vessel cylinders and the tank were automatically contoured and the known true F-18 activities were assigned to the vessels and tank volume. The CT-based model was then convolved with a 3D Gaussian PET point spread function to create the simulated phantom. For both simulated and physical phantoms, PVC was applied to recover the F-18 uptakes using a 3×3 geometric transfer matrix (GTM) method. Recovery coefficients of the vessels were calculated before and after PVC.

***Results and Discussion*:** Severe underestimations in vessel uptake were observed for both simulated and physical phantoms before PVC. After PVC the vessel uptakes recovered closer to the true uptake values. For the simulated phantom, complete PVC recovery was achieved for all vessel sizes with an accuracy $<0.2\%$. For the physical phantom, the PVC recovery was $<5\%$ for all vessel sizes except for the smallest vessel (4.8 mm), where the vessel uptake was overestimated by 20%. In conclusion, non-invasive PET image based simplified kinetic analysis is feasible provided that partial volume corrections are applied to recover vessel tracer uptake. Blood activity may be corrected for partial volume error with better than 5% accuracy using the GTM method for vessels larger than 10 mm in diameter. A patient study is needed to confirm these results in clinical settings.

Key words: Blood activity; Simplified kinetic analysis; Partial volume correction; Recovery coefficient.

Creation of 3D Histology Volume Using Image Registration Techniques

Rushin Shojaii[1,2], Tigran Karavardanyan[1], Martin Yaffe[1,2], Anne L. Martel[1,2]

[1]Imaging Research, Sunnybrook Health Sciences Centre, Toronto, ON, Canada, M4N 3M5

[2]Departments of Medical Biophysics, University of Toronto, Toronto, ON, Canada, M4N 3M5

E-mail: rushin.shojaii@utoronto.ca

The aim of this work is to propose a practical pipeline to reconstruct a 3D histology volume and register it with volumetric MR images. This work enables us to correlate histology to the findings in medical images, such as apoptotic and necrotic regions and contrast enhanced vascularised regions, using molecular contrast agents. We also report on the accuracy of this pipeline for histology volume reconstruction and the correlation of the histology volume to MR volume by calculating the target registration error using fiducial markers.

***Introduction*:** A point-based image registration pipeline is evaluated in this work for correlating histology to MR images. First, the histology volume is reconstructed. Registering the histology images to one another without reference images propagates the registration error and changes the actual shape of the histology volume. We have used optical images of the surface of the paraffin block before each section is cut as reference images to eliminate this effect. This pipeline is validated by measuring the Target Registration Error (TRE) using multi-modality fiducial markers, which are detectable in histology, the reference images and medical images.

***Materials and Methods*:** A xenograft of human breast cancer cell line (MDA) in a SCID mouse was excised and the fiducial markers, which are catheters filled with cuttlefish ink and flour and water, were implanted in the fixed tissue. The tissue was then placed in a petri dish using 3% agarose to image it at a 3T MR scanner. After MR scanning, the histology sections were cut to a thickness of 5 μm and 20 μm separation. Blockface images of the surface of the paraffin block were also captured

before each section was cut. The sections were stained with H&E and then digitized with 0.5 µm resolution.

The registration of the pairs of H&E and their correspondent blockface images was initially done using Fourier Descriptors (FDs) and then refined by Iterative Closest Points (ICP) algorithm. Thin-plate splines were used to compensate for the deformation of the histology sections due to tissue processes. The MR volume was then registered to the blockface volume using the same methods. TRE was then calculated to assess the accuracy of each step of the proposed method.

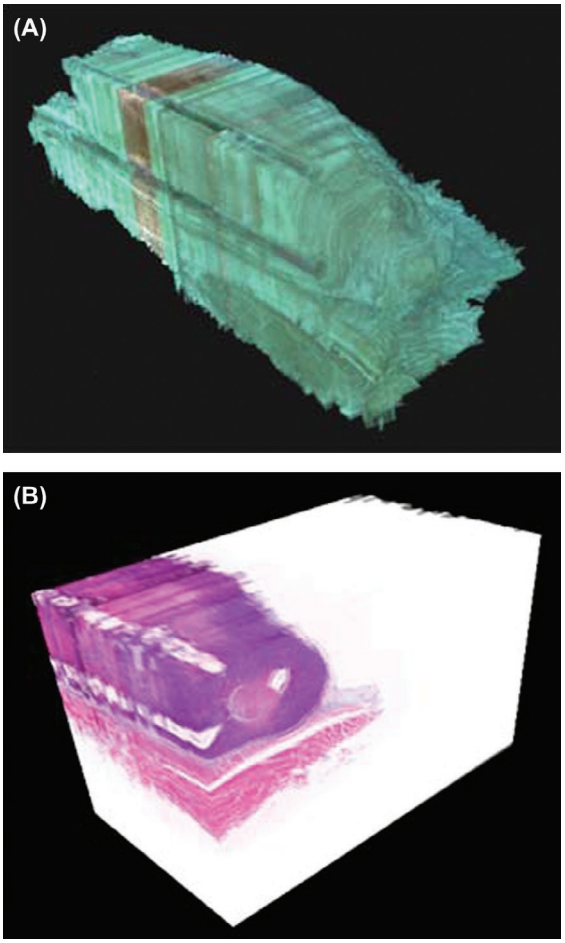

Figure 1: (**A**) Blockface volume and (**B**) Histology volume.

***Results and Discussion*:** Before alignment, TRE between the centroids of the fiducial markers in the histology images and their correspondent blockface images was 15.00 mm (Figure 1). After initial rigid alignment the TRE is 0.2 mm (standard deviation = 0.14 mm), and 0.12 mm (standard deviation = 0.19 mm) after refinement using ICP. After deformable registration the TRE is measured as 0.14 mm (standard deviation = 0.12 mm) when the stiffness value is set to zero and 0.14 mm (standard deviation = 0.12 mm) when the stiffness value is set to 1.00. These preliminary results are encouraging. Further work to improve deformable registration is needed; in particular we will use internal features as additional landmarks. The TRE for registration of MRI to the corresponding histology image will be also measured in future.

Key words: Co-registration; Histology; Magnetic resonance imaging, Image registration; Correlation.

Photoacoustic Spectral Characterization of Perfluorocarbon Droplets

Eric Strohm[1], Ivan Gorelikov[2], Naomi Matsuura[2], Michael Kolios[1]

[1]Ryerson University, Department of Physics, Toronto, Ontario, Canada, M5B 2K3

[2]Imaging Research, Sunnybrook Health Sciences Centre, Toronto, Ontario, Canada, M4N 3M5

E-mail: mkolios@ryerson.ca

***Introduction*:** Perfluorocarbon droplets are currently being investigated as agents for imaging and cancer therapy. Droplets loaded with optical absorbing nanoparticles can be used as photoacoustic contrast agents to enhance vessel and tumour visualization. Alternatively, droplets can be vaporized to gas bubbles under laser irradiation for cancer therapy by vessel occlusion and targeted drug delivery.

***Materials and Methods*:** Micron-sized perfluorocarbon droplets containing 10 nm diameter silica-coated lead sulphide nanoparticles were characterized using a scanning photoacoustic/acoustic microscope. Individual droplets were measured using photoacoustics under optical guidance. For photoacoustic measurements, droplets were irradiated with 532 and 1064 nm laser pulses focused to a 4-10 µm spot size with energies up to 450 nJ per pulse. A pulse repetition frequency of 2 kHz was used, and up to 200 signals were averaged for each measurement.

***Results and Discussion*:** This research demonstrates a method to selectively image and vaporize droplets based on laser energy or wavelength. The measured photoacoustic signal increased with increasing laser energy until droplet vaporization occurred at 200-450 nJ/pulse. The large range could be due to variations of the nanoparticle concentration within the droplets. In addition, the droplet size in a region can be estimated by comparing the signal to photoacoustic theory. In previous studies, the droplet photoacoustic signals in both the time and frequency domains differed from

theoretical predictions. Measurements of the sound speed of the perfluorocarbon liquid found an increase of 2-5% over the frequencies used. The photoacoustic theory was modified to account for the increase in sound speed, and better agreement between theory and experiment was observed by accounting for sound dispersion.

Key words: Photoacoustic; Droplet; Perfluorocarbon.

Discrimination of Benign and Malignant Breast Lesions Using Quantitative Ultrasound

Hadi Tadayyon[1,2], Lauren Wirtzfeld[3], Gregory J. Czarnota[1,2]

[1]Imaging Research and Radiation Oncology, Sunnybrook Health Sciences Centre, Toronto, ON, Canada, M4N 3M5

[2]Departments of Radiation Oncology and Medical Biophysics, University of Toronto, Toronto, ON, Canada, M4N 3M5

[3]Ryerson University, Department of Physics, Toronto, Ontario, Canada, M5B 2K3

E-mail: hadi.tadayyon@sunnybrook.ca

***Introduction*:** Emerging novel techniques for monitoring tumor response to breast cancer therapy incorporate the use of B-mode images obtained by clinical scanners due to their wide availability, portability, and short scan time. Conventional B-mode scanners (in the clinical frequency range of 1 to 10 MHz) can resolve structures on the order of hundreds of micrometers in scale, but alone cannot differentiate between benign tissues and malignant tumors. The ability to differentiate tissue type requires characterization of scatterers inside tissues, which can be achieved through the analysis of frequency dependent backscatter. We developed a tissue characterization technique for cancerous breasts using ultrasound parameters derived from backscatter frequency spectra as well as envelope statistics. The algorithm will be tested to identify tumors and track responses to neoadjuvant chemotherapy.

***Materials and Methods*:** Radio-frequency backscatter data were collected from 50 (and counting) volunteer patients prior to the start of their chemotherapy treatment, of which six have been analyzed to date. A reference phantom was constructed and imaged by the same ultrasound system to be used to calibrate the power spectrum from patient data. With the help of an oncologist (G.J.C.), two regions of interest (ROI) were selected in each breast image – healthy tissue and suspicions lesion. In each ROI, two types of analyses were performed – frequency content and envelope statistics. For frequency content analysis, the calibrated power spectrum of each ROI was computed and a line was fit to the −6 dB bandwidth. From the best fit line, three parameters were computed: midband fit, spectral slope, and 0 MHz intercept. For statistical analysis, skewness, kurtosis, and the shape parameter of the fitted generalized gamma distribution were computed for each ROI.

***Results and Discussion*:**

	Midband fit (dB)	Slope (dB/MHz)	Intercept (dB)	Skewness (au)	Kurtosis (au)	Shape parameter (au)
Lesion	−1.43	0.89	−6.40	0.82	3.86	1.33
Tissue	8.48	−0.17	9.39	0.92	4.10	0.09
Confidence level	6/6	4/6	6/6	2/6	2/6	5/6

The confidence level indicates the fraction of patients that agreed with the direction of relative change in the parameter estimated by the average. The preliminary results suggest that midband fit and intercept values are higher in tissue ROIs than lesion ROIs and the shape parameter is greater in lesion ROIs than in tissue ROIs.

Key words: Quantitative ultrasound; Breast cancer; Tissue characterization.

Enhancing Laser Thermal-Therapy Using Ultrasound-Microbubbles and Gold Nanorods: *In Vitro* Investigation

Christine Tarapacki, Carl Kumaradas, Raffi Karshafian

Ryerson University, Department of Physics, Toronto, Ontario, Canada, M5B 2K3

E-mail: ctarapac@ryerson.ca

***Introduction*:** Gold nanorods (GNRs) in laser-induced thermal therapy can significantly increase light absorption and consequently local temperature causing irreversible cell damage. However, the uptake of gold nanorods in the target tissue is limited. In this study, sonoporation – the phenomenon where ultrasound and microbubble exposure increases

the permeability of cell membranes and allows delivery of macromolecules which otherwise would be excluded – is investigated to improve uptake of gold nanorods and therapeutic outcome of laser-induced thermal therapy.

***Materials and Methods*:** Cells in suspension (acute myeloid leukemia – AML) of 0.6 mL were treated with ultrasound and microbubbles (USMB) at 1 MHz frequency, 16 microseconds pulse duration, 1 kHz pulse repetition frequency, 30 s insonation time, varying acoustic pressures (0, 1.6 and 3.1 MPa) and Definity agent (10 microlitre) with and without gold nanorods (12 nm × 48 nm) at varying concentration (1×10^{10} to 30×10^{10} GNR/mL). The GNRs were manufactured through wet chemical synthesis process and measured using TEM (transmission electron microscopy). Following ultrasound treatment, cells were centrifuged to remove excess gold nanorods and treated with 810 nm laser at an energy fluence of 1.5×10^7 J/m^2 (Diomed 60 NIR) for 5 minutes. The temperature was measured during laser treatment using a thermal camera (FLIR Thermovision A40). Cell viability was assessed using flow cytometry and propidium iodide. Cells were imaged using TEM.

***Results and Discussion*:** Ultrasound and microbubbles improved therapeutic efficacy of laser thermal-therapy. Cell viability of 18 ± 2% was achieved with GNRs+USMB (1.6 MPa) compared to 72 ± 3% with GNRs alone (12 hour incubation). Cell viability with USMB alone was 99 ± 0.2%. Cell viability decreased and temperature increased with GNRs concentration. Cell viability decreased from 92% at 1.0×10^{11} GNR/mL concentration to 29% at 1.5×10^{11} GNR/mL concentration with corresponding temperatures of 50°C and 54°C, respectively. TEM images showed uptake of GNRs in AML cells using ultrasound and microbubbles. The combined treatment of ultrasound-microbubble and gold nanorods with laser therapy showed a synergistic enhancement in cell death of *in vitro* cells. Future work will continue to investigate this effect *in vitro* and *in vivo*.

Key words: Gold nanorods; Microbubbles; Thermal therapy; Ultrasound.

Personalized Cancer Care

Maureen Trudeau[1], Gregory J. Czarnota[1], Michael C. Kolios[2]

[1]Sunnybrook Health Sciences Centre, Toronto, ON, Canada, M4N 3M5

[2]Ryerson University, Toronto, ON M5B 2K3

E-mail: maureen.trudeau@sunnybrook.ca

Personalized cancer medical therapy can takes two forms: "predictive" therapy and "adaptive" therapy. Predictive therapy is based on prognostic factors that have been related to outcomes. In this form of therapy, tumour factors such as histological grade or specific biomarkers can play a role in therapy-administration decisions. For instance, in breast cancer the presence of absence of the estrogen receptor overexpression, or Her-2-Neu overexpression, guide the administration of drugs like tamoxifen or herceptin, respectively. This principle has recently been expanded to giving women with triple negative (ER-, PR-, Her2Neu-) breast cancer different classes of chemotherapeutic drugs due to the nature of their aggressive disease. In contrast, adaptive therapy is based on monitoring responses and modifying treatment based on treatment efficacy. However, there is no good objective method yet for assessing early responses to cancer chemotherapy through the use of standard imaging methods.

For example, breast cancer is the most common malignancy for females in North America. Approximately 5-15% of the estimated 200,000 new cases diagnosed each year will present with locally advanced breast cancer (LABC). Women with LABC have a very poor outcome in terms of both local and systemic recurrence. Standard treatment for these patients is now usually neoadjuvant systemic (chemotherapy or less frequently endocrine therapy) followed by surgery and radiotherapy. However, LABC treatment remains controversial because determining the optimal treatment paradigm is fraught with uncertainties, both in terms of treatment regimen and duration of treatment. While complete pathological response to neoadjuvant chemotherapy has been shown to strongly correlate with patient survival, conventional clinical surrogates based on anatomical information such as on-going physical assessment, mammography and standard clinical imaging such as ultrasound suffer from an inability to objectively assess treatment response early during the course of treatment.

In order to assess response to treatment it is important to know the extent of initial disease. In this regard, magnetic resonance imaging (MRI) has shown promise as a staging

tool that can accurately determine the extent of cancer when compared to pathology specimens. In particular, contrast-enhanced MRI has been proven to consistently detect residual disease. Another functional imaging technique, positron-emission tomography (PET), has been reported to identify tumor changes as early as 8 days following treatment. However, both approaches can be costly. Furthermore, PET and MRI require the use of exogenous contrast agents and employ lengthy scan times that are often unfeasible for ongoing monitoring of late-stage cancer patients. Hence, alternative modalities are needed that can provide rapid and quantitative functional information about the extent of disease without the requirement of exogenous contrast agents would be of considerable value for evaluating responses to neoadjuvant therapy. It is important to know if tumours, and by inference dispersed cancer cells, are responding to neoadjuvant chemotherapy, so that an ineffective therapy could be changed to an effective therapy. Newer methods based on ultrasound and optical method provide great promise in regards to treatment monitoring and include quantitative ultrasound, elastography, diffuse optical spectroscopy, optical coherence tomography and photoacoustics. These methods provide functional images of tumour metabolism or physical properties that are being recognized to change with responses to chemotherapy and provide promise as new methods to guide neoadjuvant chemotherapy treatments.

Key word: Therapy response monitoring.

A Flexible Ultrasound Scanner for Capturing Ultrasound Images and Data at Low- and High-Frequencies

Corina Bilan-Tracey, Kris Dickie, Reza Zahiri, Corina Leung

Ultrasonix Medical Corporation, Vancouver, BC, Canada, V6V 2K9

E-mail: kris.dickie@ultrasonix.com

***Introduction*:** Today, there exists a void in the device space for a tool that can capture high-quality ultrasound images as well as raw data, for both clinically approved imaging, as well as pre-clinical and highly sought-after higher frequency imaging. Because of this, technologies developed in the pre-clinical environment, have had greater difficulty in transitioning to the clinical space. With the developments of PC based medical devices, as well as smaller and less costly technologies, the void is on its way to be being filled. With the purpose of creating superior imaging devices and a more flexible data collection interface, Ultrasonix has leveraged technology that allows higher sampling rates and bandwidths to enable low- and high-frequency imaging for both clinical and pre-clinical segments, on a single device. Standard high-frequency imaging devices are in the range of 50 to 80 Mhz, and offer high resolution and detailed images, however images and data captured between 20 and 40 Mhz offer higher resolution than conventional ultrasound with very little trade-off.

***Materials and Methods*:** The SonixTOUCH Research system offers the ability to acquire large cineloops of various types of data, ranging from raw RF signal in B-Mode, Color, PW, 3D/4D modes or scan converted data, 8-bits or 16-bits envelope data. System sequences can be manually programmed toacquire corresponding data; for example, to acquire full frames of pre-scan converted data in near real-time. An open software platform provides flexibility that can be used in conjunction with a SonixDAQ unit to enable parallel data acquisition for ultrasound research. A SonixDAQ acquires pre-beamformed RF digital data from each channel on the ultrasound system. Access to this data allows scientists to create new beamforming techniques, research new scanning methods, develop photo-acoustic applications, and discover new methods for pathology detection for research purposes. The SonixDAQ combined with the Texo SDK allows for parallel data capture and full transmit and beam sequencing capabilities. Programmability includes time-gain curves, analog filters, analog gain, acquisition depth channel masking for increasing capture time, options in standalone operation or synchronizing with the SonixRP system manual trigger and a free run mode option.

***Results and Discussion*:** Ultrasonix provides the most flexible research platform available today. New technologies such as elastography imaging, which was developed on the research platform and first used in research studies, have proven to have clinical value and have been integrated on our ultrasound systems. Ultrasonix hosts a dedicated online Research user group that provides hundreds of posts with very helpful resources such as Matlab, Python, C Code to configure the system and process data. In addition, we develop multiple toolkits and software to make the life of a researcher more efficient.[1]

Key words: Ultrasound; High-frequency; Research; Pre-clinical; Radio-frequency.

[1]Visit our library (registered research users only).

Non-Rigid Registration of DTI and Histology for Prostate Cancer Diagnosis

Carlos Uribe Munoz[1], Edward C. Jones[3], Silvia D. Chang[4], S. Larry Goldenberg[2,5], Kyzyl Herzog[1], Piotr Kozlowski[1,2,4,5]

[1]University of British Columbia, MRI Research Centre, Vancouver, BC, Canada, V6T 1Z3

[2]Vancouver Prostate Centre, Vancouver, BC, Canada, V6H 3Z6

[3]Pathology and Laboratory Medicine, University of British Columbia, Vancouver, BC, Canada, V6T 1Z7

[4]Radiology, University of British Columbia, Vancouver, BC, Canada, V5Z 4E3

[5]Urologic Sciences, University of British Columbia, Vancouver, BC, Canada, V5Z 1M9

E-mail: carluri@phas.ubc.ca

***Introduction*:** Diffusion Tensor Imaging (DTI) has shown promise in prostate cancer diagnosis (1). However, proper assessment of the accuracy of DTI as a diagnostic technique requires validation against histology of prostatectomy specimens. To make such validation objective, accurate registration of DTI and histology images is needed. Here, we present preliminary results obtained with software developed in our laboratory to register histology whole mount sections (WMS) to DTI images.

***Materials and Methods*:** MRI T2W and DTI images were obtained with a 3T Philips Achieva MRI scanner from patients with biopsy proven carcinoma prior to radical prostatectomy procedure. The excised glands were fixed for at least 24 hrs and *ex vivo* DTI images were acquired with a 7T Bruker Biospin MRI scanner. Following *ex vivo* MRI, the specimens were cut into 4 mm slices using a custom built slicing device (5), and further processed for histological analysis. Tumour areas were manually outlined by a pathologist under microscope, and digital images were generated from the annotated glass slides using a flatbed scanner. Non-rigid registration procedure composed of an affine transformation and a third order b-spline (6) was used to register the whole mount sections (WMS) to the *ex vivo* DTI images. WMS and *in vivo* DTI were both registered to *in vivo* T2W images. The inverse of the DTI registration was then applied to the registered WMS in order to match the unregistered (unmodified) FA and ADC maps calculated from the *in vivo* DTI data.

***Results and Discussion*:** 26 slices were registered and the quality of the overlap was evaluated using the Dice Similarity Coefficient (DSC). A mean DSC of 0.97 ± 0.02 and 0.95 ± 0.04 for *ex vivo* and *in vivo* was obtained respectively. Comparison of fine anatomical details between the registered images was done using an overlay with varying transparency. Three slices were excluded from the analysis based on poor match of these details. Average values of ADC and FA in regions of tumours with Gleason Score of 3+3 and 3+4, normal peripheral zone, and normal peripheral zone with enlarged glands were calculated from the registered images. Similar ROIs were manually selected on the original images, and the average ADC and FA calculated and compared to those from the registered images. Percentage differences between the two values are shown in the table below. The potential reasons for some of these differences being relatively high are tumour heterogeneity, small cancer infiltrations marked by the pathologist that cannot be detected by MRI, lower resolution in the *in vivo* DTI, and lack of proper correspondence between location and orientation of MRI and histology slices.

	%diff ADC *ex vivo*	%diff FA *ex vivo*	%diff ADC *in vivo*	%diff FA *in vivo*
Tumour GS = 3+3	3.3	0.2	15.9	17.7
Tumour GS = 3+4	13.9	0.7	13.9	23.1
Normal peripheral zone	1.8	0.8	0.3	5.3
Normal peripheral zone with enlarged glands	0.2	4.9	2.9	12.6
Average peripheral zone	5.1	2.8	0.5	9.1

Key words: DTI; Image registration; Prostate cancer.

References

1. Kozlowski, P., *et al. Magn Reson Imaging 28*, 621 (2010).
2. Gürses, B., *et al. Eur Radiol 18*, 716 (2008).
3. Manenti, G., *et al. Invest Radiol 42*, 412 (2007).
4. Xu, J., *et al. Magn Reson Med 61*, 842 (2009).
5. Drew B., *et al. J Magn Reson Imaging 32*, 992 (2010).
6. Klein, S., *et al. IEEE Transactions on Medical Imaging 29*, 196 (2010).

A High-Frequency Platform for Small Animal Ultrasound and Photoacoustuics

Desmond Hirson, Jim Mehi

VisualSonics, Toronto, ON, Canada, L6K 3L3

E-mail: dhisrson@visualsonics.com

***Introduction*:** VisualSonics is North America's premier manufacturer of high-frequency ultrasound equipment for cancer therapy monitoring. Our Vevo system provides researchers the opportunity to monitor tumor treatments in a number of manners including tumor size, tumor volume, tumor blood flow and through the quantification of biomarkers. Our newest technology the VevoLAZR further permits the co-registration of functional and structural data by permitting the collection of anatomical, function, physiological and molecular data acquisition.

***Materials and Methods*:** The Vevo system has the ability to detect tumors before they are palpable and allows for precise and accurate detection of early tumors. The Vevo system allows for exact measurements to be recorded and for the morphology to be precisely outlined. As a non-invasive imaging system, it also permits researchers to monitor progression of tumor burden over time. Examples of tumor models studied longitudinally include: TRAMP prostate, pancreatic ductal adenocarcinoma (KPC), mammary (4T1, 67NR), hepatocellular carcinoma and many others. VisualSonics 3D visualization and segmentation tools allow high-resolution 3D rendering of an area of interests at resolution down to 30 microns. Users can also apply segmentation algorithms to determine the volume of the orthotopic tumor *in vivo* and follow the progression or regression of tumor volume longitudinally. Power and Color Doppler functionality allows the identification and measurement of blood flow in and around tumors. Furthermore, relative tumor perfusion can also be quantified using Untargeted Vevo MicroMarker® contrast agents. The Vevo system can also directly quantify tumor neovasculature. Possibilities include quantification of VEGFR2 and Integrin expression, *in vivo*, by utilizing Target-Ready contrast agents.

For interventions, the Integrated Rail System and Image-Guided Needle Injection System are easily mounted, prepared, and operated. Precision adjustments are easily made to ensure that the probe, the injection system, and the mouse table are all in alignment to most effectively ensure a successful procedure. The Integrated Rail System allows the precise position of a needle/syringe to be mounted and the animal to be carefully positioned on a heated table. Injections can be performed without having to perform any surgically invasive procedure, eliminating invasive surgical procedures and consequently allows for improving animal survival rates.

Our newest technology, the Vevo® LAZR Photoacoustic Imaging System, inherently co-registers structural and functional data, simultaneously collecting and displaying high-resolution micro-ultrasound and photoacoustic signals. Applications include: The quantification of oxygen saturation and hemoglobin content, measurements of microvascular hemodynamics in real-time, molecular and cellular imaging, 2D volumetric acquisition and multiplexing.

***Results and Discussion*:** VisualSonics hardware provides high-resolution and high-quality imaging engineering for use in the study of cancer biology. Multiple imaging modes permit structural information to be coupled to functional information which can include molecular imaging, tumor perfusion, or new modalities such as photoacoustics.

Key words: Ultrasound; High-frequency; Research; Pre-clinical; Photoacoustics.

Towards a More Accurate Understanding of Tumor Response in Breast Cancer Therapy Through Registration of Ultrasound Imaging and Whole-Mount Breast Histopathology

Roxana M. Vlad[1], Navid Samavati[2], Sara Iradji[3], Michael C. Kolios[4,5], Gregory J. Czarnota[3,5], Kristy Brock[1,2,5]

[1]Radiation Medicine Program, Princess Margaret Hospital, 610 University Ave. Toronto, ON, Canada, M5G 2M9

[2]Institute of Biomaterials and Biomedical Engineering, University of Toronto, Toronto, ON, Canada, M5S 3G9

[3]Imaging Research and Radiation Oncology, Sunnybrook Health Sciences Centre, Toronto, ON, Canada, M4N 3M5

[4]Department of Physics , Ryerson University, 350 Victoria Street, Toronto, Ontario M5B-2K3

[5]Medical Biophysics, University of Toronto, Toronto, ON, Canada, M4N 3M5

E-mail: Roxana.Vlad@rmp.uhn.on.ca

***Introduction*:** Currently, the assessment of early tumor response to cancer therapy with the available routine imaging modalities is limited. Ultrasound methods that are capable of characterizing cell death following cancer therapies have been developed using quantitative ultrasound (QUS) algorithms.

These methods were validated in cancer mouse models by registration of 3D ultrasound with whole-mount tumor histopathology. The aim of this project is to extend these methods to clinical data, specifically to breast cancer patients treated with chemotherapy, and examine whether QUS methods can distinguish responders from non-responders earlier in the course of their treatment.

***Materials and Methods*:** Quantitative ultrasound (5-14MHz) and MRI are used to monitor treatment effects in a cohort of women (N = 50) treated with neoadjuvant chemotherapy for locally advanced breast cancer. Following surgery, the mastectomy samples are whole mounted using previously established protocols. The pathology slices stained with hematoxylin and eosin are digitized and reconstructed in a 3D volume. The tumors and the regions of cell death are contoured on each imaging data set and on the histological images. Each set of contours are converted to a volumetric mesh and the appropriate material properties assigned. The volumetric meshes are registered using a biomechanical model-based deformable registration algorithm (Morfeus).

***Results and Discussion*:** Preliminary data indicate that cell death following treatment may be detected as early as one week after the administration of chemotherapy in breast cancer patients. A shrinkage of approximately 20% of the reconstructed pathological volume could result following the fixation and staining protocols. Techniques to correct for this shrinkage, digitize and reconstruct histopathological images, import all data sets into a radiotherapy planning system, contour areas of cell death and rigorously compare the regions of cell death on pathological images with those regions defined as responding in imaging data sets, using deformable registration algorithms, have been developed in cancer mouse models, Figure 1.

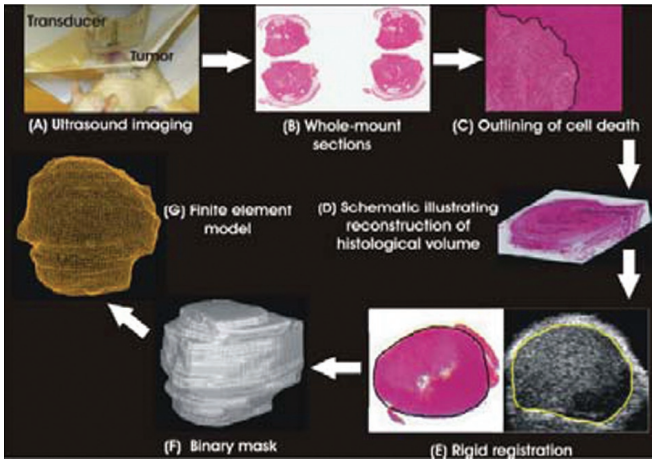

Figure 1: Flow chart illustrating the main steps of the process: (**A**) ultrasound data collection; (**B**) histological sections of a whole tumor mounted on a slide; (**C**) outlining of cell death on a histological section; (**D**) reconstruction of a histological volume by aligning consecutive slides; (**E**) registration of histological and ultrasound images and delineating a tumor on ultrasound and histological images; (**F**) contours conversion to a binary mask and (**G**) conversion of a mask file to a finite element model.

The project provides metrics of comparison between the volume of cell death assessed from gold standard-histology and that assessed from ultrasound and MRI images in breast cancer patients. The ultimate goal is to provide a means by which the effectiveness of therapies can be assessed non-invasively and integrate these findings into the current clinical practice.

Key words: Ultrasound; Tumour response; Biomechanical based deformable registration.

Novel Methods in Quantitative Pathology

Martin J. Yaffe[1,2], Gina Clarke[1]

[1]Imaging Research, Sunnybrook Research Institute, Toronto, ON, Canada, M4N 3M5

[2]Departments of Medical Biophysics and Medical Imaging, University of Toronto, Toronto, ON, Canada, M4N 3M5

E-mail: martin.yaffe@sri.utoronto.ca

***Introduction*:** Over the past twenty years, *in vivo* medical imaging techniques have almost entirely become digital, largely due to the increased flexibility of image display, access to quantitative information, more efficient archiving and retrieval and the facility to transmit and share images between different locations. A similar trend is beginning to occur in pathology. This is motivated in part by the increasing interest in quantifying biomarkers of disease and the development and application of sophisticated image analysis techniques.

***Materials and Methods*:** In this presentation three specific areas of research effort will be described. The first is in the development of whole-mount histopathology for the purposes of improved accuracy of assessing tumour margins and multifocality of disease as well as for more comprehensive correlation of *in vivo* and pathology information. It is also possible to create quasi three-dimensional image data sets and to evaluate tumour volume from such images. The second focus is on the development and evaluation of techniques that allow spatial co-localization of multiple cancer biomarkers. Such tools can be of great value in shedding light on mechanisms of cancer progression and in characterizing disease to guide the choice of more individualized treatment regimens. Finally, examples will be given of computer-assisted techniques which could be used to facilitate or improve the accuracy of pathology assessment.

***Results and Discussion*:** Examples of the use of these techniques as applied to several cancer sites will be presented and

their role in facilitating the development and validation of new *in vivo* imaging methods will be discussed.

Key words: Pathology; Biomarkers; Quantitative imaging.

Imaging Speckles: From High Frequency Ultrasound to Optical Coherence Tomography

Victor Yang

Ryerson University, Department of Physics, Toronto, Ontario, Canada, M5B 2K3

E-mail: victor.xd.yang@gmail.com

We observe the overlapping length scale between high frequency ultrasound and optical coherence tomography, and the common theme of speckle in both imaging modalities as affected by motion. Image processing algorithms and hardware platforms specifically designed to distinguish motion can obtain physiologically relevant information in animal models, with the future potential to perform clinical imaging.

We will review the results to-date on speckle-based motion detection schemes in high frequency ultrasound and optical coherence tomography and discuss their applications in therapeutic monitoring.

Ultrasound and Microbubble Mediated Sonoporation: Effect of Cell Membrane Cholesterol Content on Cell Permeability and Cell Viability

Tetyana Yatsenko, Carl Kumaradas, Raffi Karshafian

Ryerson University, Department of Physics, Toronto, Ontario, Canada, M5B 2K3

E-mail: tyatsenk@ryerson.ca

***Introduction*:** The application of ultrasound with microbubbles – a shell-encapsulated gas-core bubble with a diameter of 1-5 μm, has been shown to increase cell membrane permeability and allow molecules, which otherwise would be excluded, to enter the intracellular space of cells; this phenomenon is referred to as *sonoporation*. The primary mechanism underpinning sonoporation has been shown to be the formation of non-lethal and transient disruptions on the cell membrane. In addition to the transient membrane disruption mechanism, endocytosis, which is a biological internalization process, has been shown to facilitate intracellular delivery at low ultrasound exposure conditions. Sonoporation efficiency, which refers to the percentage of cells that have been reversibly permeabilized, varies significantly between studies. The heterogeneity in sonoporation efficiency can be partly accounted for by different experimental conditions including ultrasound and microbubble exposure parameters and effects associated with experimental apparatus, and by the biomechanical properties of cells. In this study, the effect of cell membrane composition, cholesterol content in particular, on the ability of ultrasound and microbubbles to permeabilize cells while maintaining viability was investigated in an *in vitro* cell model.

***Materials and Methods*:** Cell plasma membrane cholesterol content was modified with methyl-beta-cyclodextrin (cholesterol depletion) and cholesterol- methyl-beta-cyclodextrin (cholesterol loading). Cells in suspension were exposed to ultrasound and microbubbles. Following the ultrasound treatment, cell permeabilization was assessed with FITC-dextran fluorescent molecule (70 kDa). Cell viability was assessed using flow cytometry and propidium iodide, which stains cells whose membrane integrity has been compromised. Experiments were performed on two cell lines: breast cancer (MDA-MB-231) and prostate cancer (PC3) cells.

***Results and Discussion*:** Ultrasound and microbubble induced permeabilization of cells depend on the cholesterol content in the plasma membrane. Cell permeability of the MDA-MB-231 cells with unmodified plasma membrane was measured to be 30% comparing to 15% for cholesterol depleted cells at 1.5 MPa peak negative acoustic pressure. Viability for unmodified and cholesterol depleted MDA-MB-231 cells at 1.5 MPa was 66% and 40% respectively. This study identified a dependence between sonoporation efficiency and the cholesterol content of plasma membrane. Cholesterol depleted cells were easier to permeabilize, as well as to kill, compared to unmodified cells. This knowledge may help to improve efficiency of ultrasound-and-microbubble mediated targeted drug delivery.

Key words: Sonoporation; Plasma membrane cholesterol; Methyl-beta cyclodextrin; Plasma membrane permeabilization; Cell viability.